TKK Dissertations 62
Espoo 2007

ELECTRICAL CHARACTERIZATION OF NITROGEN CONTAINING III-V SEMICONDUCTORS

Doctoral Dissertation

Victor Tapio Rangel Kuoppa

Helsinki University of Technology
Department of Electrical and Communications Engineering
Micro- and Nanosciences Laboratory

TKK Dissertations 62
Espoo 2007

ELECTRICAL CHARACTERIZATION OF NITROGEN CONTAINING III-V SEMICONDUCTORS

Doctoral Dissertation

Victor Tapio Rangel Kuoppa

Dissertation for the degree of Doctor of Science in Technology to be presented with due permission of the Department of Electrical and Communications Engineering for public examination and debate in Auditorium S4 at Helsinki University of Technology (Espoo, Finland) on the 9th of March, 2007, at 12 noon.

Helsinki University of Technology
Department of Electrical and Communications Engineering
Micro- and Nanosciences Laboratory

Teknillinen korkeakoulu
Sähkö- ja tietoliikennetekniikan osasto
Mikro- ja nanotekniikan laboratorio

Distribution:
Helsinki University of Technology
Department of Electrical and Communications Engineering
Micro- and Nanosciences Laboratory
P.O. Box 3500
FI - 02015 TKK
FINLAND
URL: http://www.micronova.fi/units/mns/
Tel. +358-20-722 6640
Fax +358-9-451 5008
E-mail: tapio.rangel@gmail.com

© 2007 Victor Tapio Rangel Kuoppa

ISBN 978-951-22-8637-9
ISBN 978-951-22-8638-6 (PDF)
ISSN 1795-2239
ISSN 1795-4584 (PDF)
URL: http://lib.tkk.fi/Diss/2007/isbn9789512286386/

TKK-DISS-2267

Picaset Oy
Helsinki 2007

HELSINKI UNIVERSITY OF TECHNOLOGY P. O. BOX 1000, FI-02015 TKK http://www.tkk.fi	ABSTRACT OF DOCTORAL DISSERTATION
Author Victor Tapio Rangel Kuoppa	
Name of the dissertation Electrical characterization of nitrogen containing III-V semiconductors.	
Date of manuscript December 18th, 2006	Date of the dissertation March 9th, 2007
☐ Monograph	☒ Article dissertation (summary + original articles)
Department Department of Electrical and Communications Engineering Laboratory Micro- and Nanosciences Laboratory Field of research Optoelectronics Opponent(s) Professor Patrick J. McNally Supervisor Docent Markku Sopanen (Instructor)	

Abstract

Several nitrogen containing III-V compound semiconductors, together with GaInAs and AlGaAs, were electrically characterized. The main technique used was deep level transient spectroscopy (DLTS), but also current voltage (*I-V*), capacitance voltage (*C-V*), isothermal transient spectroscopy (ITS) and Hall measurements were employed.

As a contribution to the DLTS technique, the use of inductors in DLTS was theoretically and experimentally researched. A new technique to get the real Schottky series capacitance and resistance is proposed. Its application to AlGaAs is shown.

Si-doped GaInAs and GaInNAs with small In and N content, lattice matched to GaAs, grown by molecular beam epitaxy (MBE), were studied by DLTS. Samples were studied after growth and after various thermal treatments. Several deep levels were found, and their properties (activation energy, capture cross section, density) were examined as a function of the annealing treatment. The GaInAs sample showed three deep levels, which are suspected to be related with deep levels M5, EL4 and EL10.

The GaInNAs samples with medium and heavy Si-doping were also studied. The medium Si-doped sample showed five deep levels, whose concentrations varied upon annealing temperature. The analysis suggested they are related to EL2, off-centre substitutional oxygen in As sites, clustering of GaNAs and GaInAs, intrinsic to GaAs and high disorder introduced. The heavy Si-doped sample showed one deep level, the concentration of which was reduced with increasing annealing temperature, and it is suspected to also be intrinsic to GaAs.

InN grown by metal-organic vapour phase epitaxy (MOVPE) was studied. Growth temperature strongly affects the island size, optical quality and electrical properties of the material. Several metal contacts (Au, Ag, Pt, Pd, Cu, Ni, Ge, Ti, Cr and Al) were tested and studied by *I-V*. Only Pt and Ge yielded some Schottky contact behavior, but were very unstable. Al contacts annealed at 550 ^{o}C for 1 min formed stable rectifying contacts.

Keywords Electrical characterization, DLTS, ITS, IV, CV, Hall, III-V, GaInAs, GaInNAs, InN, deep level	
ISBN (printed) 978-951-22-8637-9	ISSN (printed) 1795-2239
ISBN (pdf) 978-951-22-8638-6	ISSN (pdf) 1795-4584
ISBN (others)	Number of pages 120
Publisher TKK Micro- and Nanosciences Laboratory	
Print distribution TKK Micro- and Nanosciences Laboratory	
☒ The dissertation can be read at http://lib.tkk.fi/Diss/2007/isbn9789512286386/	

Preface

The work presented in this thesis has been carried out at the Optoelectronics Research Center of Tampere University of Technology (ORC-TUT) during 1999-2003 and the Micro- and Nanosciences Laboratory of Helsinki University of Technology during 2004-2006.

I want to express my gratitude to Professor Markus Pessa, Pirjo Leinonen, Tomi Leinonen, Janne Konttinen, Chang Si Peng, Tomi Jouhti, Suvi Karirinne, Antti Tukiainen, Emil-Mihai Pavelescu, Wei Li and Pekka Laukkanen from ORC-TUT for growth of the samples, collaboration and scientific discussion. I also want to thank Dr. James Dekker, from VTT, for helping me in the scientific analysis of the results and the preparation of manuscripts.

I also want to express my gratitude to Prof. Harri Lipsanen, Prof. Turkka Tuomi, Dr. Markku Sopanen, Dr. Mikael Mulot, Dr. Teppo Hakkarainen, Dr. Jaakko Sormunen, Dr. Lauri Knuuttila, Dr. Juha Riikonen, Sami Suihkonen, Pasi Kostamo, Marco Mattila, Outi Reentilä, Antti Säynätjoki, Aapo Lankinen, Jouni Tiilikainen, Olli Svensk, Hannu Koskenvaara, Teemu Lang, Abuduwayiti Aierken and, in general, to all the people from Micro- and Nanosciences Laboratory of Helsinki University of Technology, for scientific collaboration and discussion, sample growth, data analysis and a very friendly and fruitful environment.

I want to thank the National Council for Science and Technology (CONACYT) from Mexico, fellowship 136605, and the National Graduate School of Electronics Production Technology and Reliability, from Finland, for economical support.

I want to thank my fiancée Sujel Melina Murillo Polania for her wonderful support and charming presence during this work, and my parents Eila Hilkka Hillervo Kuoppa Salo de Rangel and Victor Fermín Rangel Fonseca, for their emotional support and encouragement.

Espoo, Finland, October 2006 Victor Tapio Rangel Kuoppa

Table of Contents

Preface v

List of publications vii

Author's contribution viii

1. Introduction 1

2. Deep level transient spectroscopy characterization of semiconductors 4

2.1 Introduction and historical background 4

2.2 Generation-recombination theory of carriers 7

2.3 Schottky contacts and its characterization by current-voltage (*I-V*) and capacitance-voltage (*C-V*) techniques 11

2.4 Deep level in the depletion region of a Schottky contact 14

2.4.1 Majority carrier trap 14

2.4.2 Minority carrier trap 19

2.5 Principles of DLTS 20

3. Use of inductors in DLTS 27

4. Electrical characterization of GaInAs 32

5. Electrical characterization of GaInNAs 37

6. Electrical characterization of InN 41

6.1 InN growth by MOVPE 42

6.2 Metal contacts on InN 45

7. Summary 49

References 51

List of Publications

This thesis consists of an overview and of the following publications which are referred to in the text by their Roman numerals.

I. Victor-Tapio Rangel-Kuoppa, Antti Tukiainen and James Dekker, *Theoretical and practical research of the use of inductors for improving DLTS characterization of semiconductors,* Microelectronics Journal **34**, 751-753 (2003).

II. V. T. Rangel-Kuoppa and M. Pessa, *Inductance deep-level transient spectroscopy for determining temperature-dependent resistance and capacitance of Schottky diodes,* Review of Scientific Instruments **74**, 4561-4563 (2003).

III. V. T. Rangel-Kuoppa and J. Dekker, *Deep levels in GaInAs grown by molecular beam epitaxy and their concentration reduction with annealing treatment*, Materials Science and Engineering B **130**, 5-10 (2006).

IV. Tomi Jouhti, Chang Si Peng, Emil-Mihai Pavelescu, Wei Li, Victor-Tapio Rangel-Kuoppa, Janne Konttinen, Pekka Laukkanen and Markus Pessa, *Group III-Arsenide-Nitride Quantum Well Structures on GaAs for Lasers Diodes Emitting at 1.3 μm*, Proceedings of SPIE **4651**, 32-41 (2002).

V. V. T. Rangel-Kuoppa and J. Dekker, *Deep levels in GaInNAs grown by molecular beam epitaxy and their concentration reduction with annealing treatment*, Materials Science and Engineering B **129**, 222-227 (2006).

VI. S. Suihkonen, J. Sormunen, V. T. Rangel-Kuoppa, H. Koskenvaara and M. Sopanen, *Growth of InN by vertical flow MOVPE*, Journal of Crystal Growth **291**, 8-11 (2006).

VII. Victor-Tapio Rangel-Kuoppa, Sami Suihkonen, Markku Sopanen and Harri Lipsanen, *Metal Contacts on InN: Proposal for Schottky Contact*, Japanese Journal of Applied Physics **45**, 36-39 (2006).

Author's contribution

The author carried out all the electrical characterization (including sample cleaning, photolithography, annealing treatment, metal deposition, etc….) except for publication IV. In publications I and II, the author took care of building an inductance box and making the deep level transient spectroscopy (DLTS) measurements with and without inductances in series. In publications III and V, the author made the current voltage (*I-V*), capacitance voltage (*C-V*) and DLTS measurements of the samples. In publication IV, the author made the atomic force microscopy (AFM) measurements. In publication VI, the author carried out the Hall measurements. In publication VII, the author made the *I-V* measurements. The author analyzed all the data of the electrical measurements. In all the articles, except for publication IV and VI, the author wrote the first version of the manuscript. In publication VI the author wrote the Hall measurement part and participated in the discussion of the manuscript.

Chapter 1

Introduction

The speed of data transmission has increased impressively in the last century. Nowadays, telecommunication is the principal way for data transmission. This has caused the appearance of the Internet and its fast growth, with all its known benefits. Nevertheless, larger capacity is still demanded every day. For example, the bit-rate requirements for local area and metro area networks have increased from 100 Mbps to 10 Gbps. To achieve these goals, quartz fiber has been used as a reliable transport media for information. Quartz fiber as an optical medium has dispersion and attenuation minima at the wavelengths of 1.3 and 1.55 μm, respectively. It also has local attenuation minima at 850 nm and 1.3 μm. These properties have fixed these wavelengths as the optical communications wavelengths. Therefore, in order to use these characteristics profitably, it is fundamental to have lasers lasing in these wavelengths.

The first approach for the 1.3 and 1.55 μm wavelengths was done by fabricating lasers using InGaAsP bulk layers and quantum well (QW) structures as the active area on InP substrates. For the 850 nm wavelength, the GaAs material has been used, due to its suitable band gap, and the possibility to grow good quality mirrors, using the well-established AlGaAs material system. This facilitates the use of vertical cavity surface-emitting laser (VCSEL), whose use has rapidly spread in the short-range optical telecommunication. Due to this there has been a lot of research in GaAs-based active materials.

Some other promising approaches have been proposed recently to improve the performance of the 1.3 and 1.55 μm lasers and to make them cheaper, such as the use of In(Ga)As quantum dot structures[1], the use of a small fraction of nitrogen to red shift the wavelength of GaAs[2] by forming GaAsN and GaInNAs[3], and recently, it has been found that the real optical bandgap of InN is in the order of 0.7 – 1.0 eV[4,5], compatible with the optical communications wavelengths. It is also worth to note that many other applications for these materials have been proposed, such as heterojunction bipolar transistors[6], high-efficiency solar cells[7-9] and photodiodes[10]. Although all these novel approaches have been intensively studied during the last two decades, there is still room for improvement in material quality.

It is well known that deep levels can play an important role in the optical properties of materials, as they can act as non-radiative recombination centers, hindering the emission of

photons, and consequently diminishing the quality of the material for making suitable lasers and other optical devices. Also, it is necessary to know the electrical properties of the material such as carrier concentration and mobility, as lasing is usually done via electrical stimulation, *i.e.*, by injecting carriers. Therefore, a thorough knowledge of the electrical properties of the material is very useful. Several techniques are used to study the electrical properties. The major ones among them are: Hall measurements, current-voltage (*I-V*) measurements, capacitance-voltage (*C-V*) measurements, and deep level transient spectroscopy (DLTS).

As the name says, DLTS is a technique for studying deep levels. Deep levels are localized energetic levels close or in the middle of the band gap. DLTS has become a powerful tool to study them: it is a practical, fast and easy technique that can distinguish between a minority and a majority carrier deep level. In the basic variant, it provides the deep level energy, capture cross section and density of deep levels. Several improved versions of the technique might yield more data: deep level profiling, photonic capture cross sections, temperature dependent capture cross sections, etc… Further details about the DLTS technique will be given in Chapter 2.

The first part of this work consists of the proposal of two techniques using inductors to improve the results that are obtained by DLTS. In publication I, the use of inductors in series with a DLTS sample is studied theoretically and experimentally for the first time, in order to improve the acquisition of data by DLTS. A resonance condition is found. It is experimentally tested and it is shown that it separates overlapping signals, making it easier to determine the position of the deep level peaks. In publication II, the use of inductors to calculate the real series resistance and capacitance of a Schottky contact is demonstrated. It is generally assumed that the series resistance of a Schottky contact is negligible, and thus, the Schottky contact only shows a capacitive nature. It is found that in practice this is not correct: the series resistance of a Schottky contact is not zero, particularly at low temperatures. The use of inductors, *via* impedance equations, yields an easy technique to calculate the real series resistance and capacitance of a Schottky contact as function of temperature, and therefore, a way to correct the spectra and obtain the real deep level parameters.

Several deep levels in n-type GaInAs, and their thermal annealing behavior are reviewed in publication III. The presence of three deep levels is reported, as well as their thermal annealing behavior. The concentration of all the three deep levels is reduced by thermal annealing.

In publication IV, lattice-matched bulk samples and several strained single and multiple QW structures of GaInNAs grown by conventional molecular beam epitaxy (MBE) are reported. The structures were studied by room temperature photoluminescence (PL), x-ray diffraction (XRD) and atomic force microscopy (AFM). It was found that the PL wavelength might blue shift up to 55 nm and the PL intensity might increase by up to 45 times, depending on the structure and thermal annealing treatment. Several deep levels in n-type GaInNAs, and their thermal annealing behavior, are studied in publication V. Up to five different deep levels are presented and their origin is discussed.

In publication VI, the growth of InN by metalorganic vapour-phase epitaxy (MOVPE) reactor on sapphire substrates is reported. The samples were studied by XRD, AFM, PL and Hall measurements. It was found that InN films consist of hexagonal islands and have a rough surface. Also, growth temperature has a strong effect on the island size, optical quality and electrical properties of the InN layer. This work connects to publication VII, in which several metal contacts (Au, Ag, Pt, Pd, Cu, Ni, Ge, Ti, Cr, Al) are tested (some for the first time) for InN. Pt and Ge show some Schottky behavior. All the other metal contacts show ohmic nature. It was also found that, if the Al contacts are annealed, a rectifying behavior appears. This is explained by an interfacial reaction between InN and Al, which forms AlInN, a semiconductor with a higher band gap than InN, between the InN and the Al contact.

The structure of this thesis is as follows. In Chapter 2 a brief overview of the DLTS technique is given. In Chapter 3 the author's contribution to the DLTS technique using inductors is presented. In Chapter 4 the electrical properties of GaInAs are briefly summarized, as well as the new results coming from publication III. The same is done for GaInNAs in Chapter 5, including results from publications IV and V. In Chapter 6 a brief description of the electrical properties of InN is presented, and some of the results of publications VI and VII are overviewed. Finally in Chapter 7 a summary of all the results is given.

Chapter 2

Deep level transient spectroscopy characterization of semiconductors

In order to understand the deep level transient spectroscopy (DLTS) technique better, first an introduction to the basic ideas of semiconductor crystals, allowed and forbidden energy states, shallow levels and deep levels is presented in Section 2.1. In the same Section, a brief historical summary is given. Next, the generation-recombination theory of carriers will be described in Section 2.2. In Section 2.3, the formation of a Schottky contact is briefly reviewed, including the current-voltage and capacitance-voltage equations. The behavior of a deep level in the depletion region of a Schottky contact, as a function of the bias, will be explained in Section 2.4. The same ideas apply for the case of p-n junctions. In Section 2.5 these two theories will be merged together with the concepts introduced by D. V. Lang to explain the principle of the DLTS method.

2.1 Introduction and historical background

Semiconductors can be modeled by assuming an infinite perfect crystal. Starting from a single atom, which has its well-defined energy levels, more and more atoms are added into a periodic array, and the eigenenergies are solved from the Schrödinger equation. This might be done with one kind of atom or several ones. As more and more atoms are taken into account, the well-defined atomic energies mix, and start to form energy bands. When finally an infinite periodic array is considered, three areas of energy appear: on the low part of the energy scale, the valence band, where the electrons localized to near-atomic states are; on the top part of the energy scale, the conduction band, for electrons with enough energy to move through the crystal; and in-between these two bands, the forbidden gap, where no electron states are allowed. The difference in energy between the bottom of the conduction band and the top of the valence band is known as the band gap. Tentatively, semiconductors are considered to have a band gap between 0 and 3 eV.

Also other materials, such as metals or insulators, can form crystals. What separates metals from semiconductors is the overlapping of the valence and conduction band. This causes a large electron population in the conduction band: hence, their good electrical and thermal conductivity. Insulators, on the other hand, have a larger band gap than semiconductors. Due to this, the electron population in the conduction band is very small, which explains their poor

electrical and thermal conductivity. It is important to note there are exceptions to these definitions[11]: there are such materials like semiconducting diamond (with an energy gap of 6 eV). GaN and AlN, which have band gaps of 3.5 eV and 6 eV, are considered semiconductors, as well.

This picture is very useful to get a first understanding of semiconductors: it helps to explain many of their electrical, structural and optical properties, such as carrier concentration, mobility, x-ray diffraction (XRD) patterns, absorption and emission of photons, and so on.

Unfortunately, this theory has two major assumptions, which are not true in the real world: there are no perfect crystals and there are no infinite crystals. The crystal quality may be affected, e.g., by structural defects: point defects, line defects, dislocations, complexes, interstitial atoms, vacancies, substitutional atoms, antisites, etc… The crystalline structure also inevitably ends at the crystal surface or at the interface to another material.

Even though one tries to fabricate a semiconductor material with only the desired constituent atoms, other atoms are always present too: they are called impurities. The impurity atoms might get into the crystal during growth or by diffusion due to structures of different kinds of materials. Metal deposition, chemical treatments, annealing or ion bombardment are also sources of these impurities. In some cases, they are incorporated deliberately. This process is known as doping. The controlled incorporation of impurities is the key for controlling carrier concentration. The impurities will then act as either donors or acceptors. Due to the presence of all these defects and impurities, some localized energy levels appear inside the band gap.

When semiconductor technology was at its first stages after World War II, only simple semiconductors were studied and used: Si and Ge. Then it was realized that doping drastically modified the electrical properties of the host semiconductor. This helped to tailor the material for the desired purpose. The overall behavior was easily understood using the hydrogenic model: this model explains the energy levels as hydrogen-like levels in the band gap, and as they are very close to the conduction and/or the valence band (just a difference in energy of 5-10 meV), they are called *shallow levels*. But as the industry continued its development, compound semiconductors appeared (GaAs, InP, etc…). As the analysis techniques developed, as well, it was realized that other energy levels, in both simple and compound semiconductors, are present. They are neither close to the conduction nor the valence band, *i.e.*, closer to the middle of the band gap, thus, they are called *deep levels* (Fig 1).

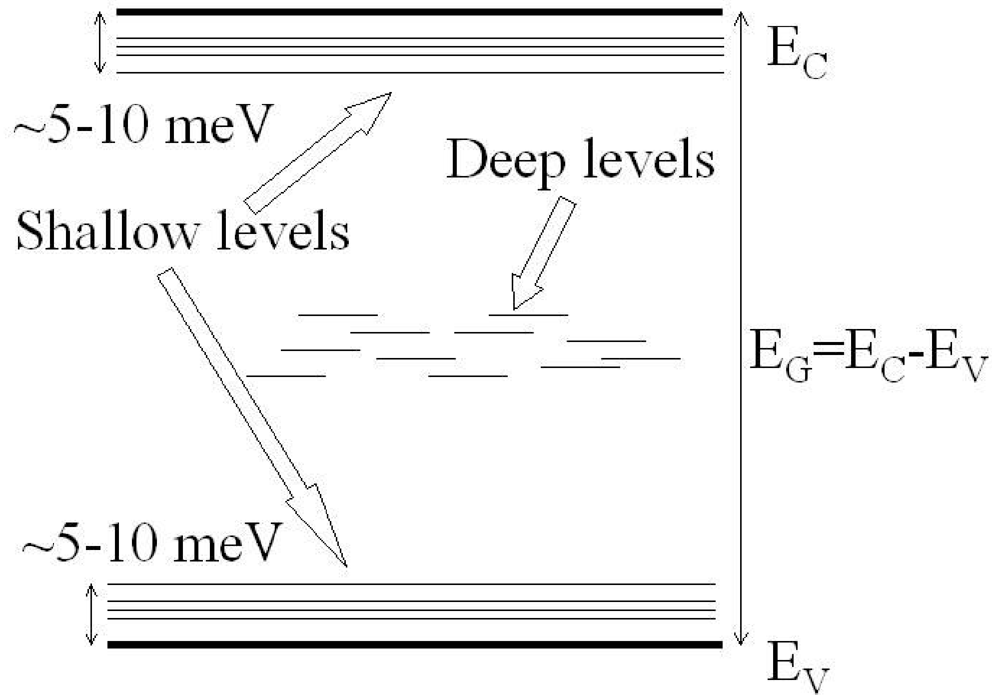

Fig. 1. Simplified image describing the position of shallow and deep levels in the band gap of a semiconductor. Note the more extended nature of shallow levels, in contrast with the more localized nature of deep levels. E_C and E_V are the conduction band and valence band energy, respectively. $E_G= E_C - E_V$ is the band gap energy.

Due to the hydrogenic behavior of the shallow levels, they are less localized compared to deep levels, and thus less sensitive to possible distortions in the immediate surrounding lattice, so they can be described in terms of fewer macroscopic parameters. This nature makes shallow levels usually radiative, therefore, luminescence provides a sensitive, fast and spectroscopic technique to study them[12].

On the contrary, deep levels in general are very localized states, and sometimes non-radiative, which causes problems for optical applications. This explains why they can only be described if both the nature of the defect and the host lattice are taken fully into account. During the fifties, sixties and the first half of the seventies, several techniques were proposed to get information about these elusive deep levels: thermally stimulated current (TSC)[13], admittance spectroscopy[14], analysis of photoconductivity rise or decay curves[15], optically stimulated conductivity[16], the dependence of space-charge-limited currents on applied voltage analysis[17]. The ingenuous idea of using the change of capacitance under bias conditions due to the refilling of deep levels was already proposed in the sixties[18]. At the beginning the refilling

was done *via* optical stimulation. Later, the change in capacitance was monitored versus an increasing temperature, which yielded the thermally stimulated capacitance (TSCAP) technique[19].

D. V. Lang realized that all these techniques lacked the sensitivity, speed, range of observable trap depths and the spectroscopic nature to make them practical for doing spectroscopy on non-radiative centers in a large number of samples. Therefore, in 1974 he proposed the deep level transient spectroscopy (DLTS) technique[20].

DLTS is based on the analysis of the change of capacitance due to a change in bias condition at different temperatures. It can be applied to Schottky contacts and p-n junctions. DLTS is not a spectroscopic technique in the sense that some parameter is monitored as a function of the frequency. Thus, there has been some discussion that the last letter "S" should be better considered to come from "scan", as the "scanning" variable is temperature. Nevertheless, the "spectroscopy" word has remained and it is known like that nowadays. It has advantages over TSC due to its better immunity to noise and surface channel leakage currents. It can distinguish between majority and minority carrier traps, unlike TSC, and has a strong advantage over admittance spectroscopy, which is limited to majority-carrier traps. Comparing with TSCAP, DLTS has much greater range of observable trap depths and improved sensitivity.

2.2 Generation-recombination theory of carriers

The generation-recombination theory explains the processes when carriers are captured or emitted between energy levels in the band gap and the conduction and valence bands[21]. It is one of the basic theories behind understanding DLTS.

For simplicity, it is assumed that there is one set of deep levels (also known as *traps*) with one single energy E_T in the band gap, and capable of capturing at most one electron each one, as shown in Fig. 2.

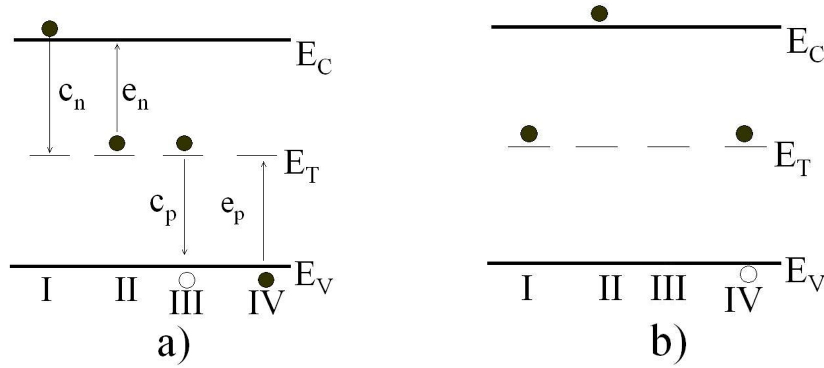

Fig. 2. Four possible recombination and generation processes a) during the process and b) after the process. Full circles represent electrons and open circles represent holes. The arrows represent the transition of an electron between different energy levels. After Ref. 21.

The processes that can happen between these deep levels and the conduction and valence band are: I) capture of an electron from the conduction band to the trap; II) electron emission from the trap to the conduction band; III) capture of a hole from the valence band to the trap (*i.e.*, emission of an electron from the trap to the valence band) and IV) hole emission from the trap to the valence band (*i.e.*, capture of an electron from the valence band to the trap) [21].

A process I followed by a process III is known as *recombination.* A *generation* process is a process II followed by a process IV. In both, recombination and generation processes, the conduction band, the valence band and the trap participate in the change of energy of the electron. Whether a deep level will act as a generation or a recombination center, depends on the location of the Fermi energy in the band gap, the temperature and the capture cross section. For example, if there is an excess of carriers in the semiconductor, they will act as recombination centers, but if the density of carriers is below its equilibrium value, they will behave as generation centers.

It is important to note the following: in this simplified case, if there is an electron in the trap, then the trap posses a negative charge. Otherwise, if there is no electron in the trap (*i.e.* it posses a hole), it is in a neutral state. Of course, other possibilities might occur: neutral and positive states, or even states that change by two electron charge units. In order to keep the following explanation simple, we maintain the assumption that the trap has a negative charge if it has an electron and, otherwise, is neutral.

It is assumed that there is a density of electrons n and a density of holes p in the semiconductor. N_T is the total density of deep levels, either with a captured electron

(*occupied*) or none (*empty*), n_T is the density of deep levels that are occupied and p_T is the density of deep levels that are empty. Clearly

$$n_T + p_T = N_T. \quad (1)$$

No other emission or capture processes than the ones described before are assumed, *i.e.*, any radiative and/or Auger processes are neglected. The time rate of change of n is given by the electrons that are emitted into the conduction band, minus the electrons that are captured from the conduction band by the deep level. The first term depends on the emission rate from the deep levels multiplied by the available electrons on the deep levels: $e_n n_T$. The second term not only depends on the available electrons in the conduction band multiplied by the capture rate, but also on the available empty deep levels that can capture them (p_T). Thus, the second term is described by $c_n n p_T$, and the overall change of n by unit of time t is given by

$$dn/dt = e_n n_T - c_n n p_T. \quad (2)$$

A similar expression is found for the time rate of change of p

$$dp/dt = e_p p_T - c_p p n_T. \quad (3)$$

The capture rates c_n and c_p are expressed by

$$c_i = \sigma_i <v_{th}>_i, \quad (4)$$

where i represents either n or p for electrons or holes, respectively, σ_i is the capture cross section and $<v_{th}>_i$ is the average thermal velocity of the free carriers.

These two equations explain how the population n_T in the deep level changes with t

$$dn_T/dt = dp/dt - dn/dt = e_p p_T - c_p p n_T - e_n n_T + c_n n p_T. \quad (5)$$

Rearranging terms and using Eq. 1

$$dn_T/dt = (c_n n + e_p)(N_T - n_T) - (c_p p + e_n) n_T. \quad (6)$$

Eq. 6 is not easy to solve, as n and p depend on time. In some cases, also c_n, e_p, c_p and e_n might depend on t, as their values might vary depending on the charge state of the deep level[22]. For example, the order of the magnitude of the capture cross section, depending on their charge state, is shown in Table I[22].

Table I. Different orders of magnitude for capture cross sections of deep levels in different electrical states. After Ref. 22.

Charge state	Order of magnitude of the capture cross section σ (cm^2)
Attractive	10^{-14}
Neutral	10^{-16} - 10^{-17}
Repulsive	10^{-19}

Nevertheless, Eq. 6 can be solved readily if three assumptions are valid: I) all the emission and capture rates are constant, II) n and p are small and/or III) n and p are constant. It will be seen in the next Subsection that these conditions happen in the depletion region of a Schottky contact. Considering these assumptions, the solution to Eq. 6 is

$$n_T(t) = n_T(0)e^{-t/\tau} + (c_n n+e_p)/(c_n n+e_p+c_p p+e_n)\, N_T(1- e^{-t/\tau}), \quad (7)$$

where $\tau =(c_n n+e_p+c_p p+e_n)^{-1}$ and $n_T(0)$ is the occupation of the deep levels at $t=0$.

After a time long enough $(t\rightarrow\infty)$ the semiconductor is in steady state and thermal equilibrium and the population of carriers is in balance. Then the value for the steady-state concentration in the deep level is

$$n_T = (c_n n+e_p)/(c_n n+e_p +c_p p+e_n)\, N_T. \quad (8)$$

Eqs. 7 and 8 will be very useful in the next Section to explain how deep levels behave in the depletion region of a Schottky contact, either in forward or reverse bias.

2.3 Schottky contacts and their characterization by current-voltage (*I-V*) and capacitance-voltage (*C-V*) techniques

In this section, the Schottky contact formation will be briefly reviewed. The properties of Schottky contacts, including the current-voltage (*I-V*) and capacitance-voltage (*C-V*) equations, are also discussed.

Fig. 3 shows the formation of a Schottky contact between a metal and a semiconductor having a deep level. A deep level with an energy level E_T below, but close to the Fermi energy E_F, is shown. It is included because it is needed during the explanation of the DLTS technique in the following sections. The full circles represent the electrons. In Fig. 3 a) the semiconductor and the metal are shown when they are separated and far from each other, depicting their different E_F, and in Fig. 3 b) it is shown what would happen if the materials were brought into contact suddenly. E_F is still different in the metal and the semiconductor, *i.e.*, there is no thermodynamic equilibrium. In order to achieve it, electrons move into the metal (arrows), where they find lower energy states, which are empty given the large density of states of metals.

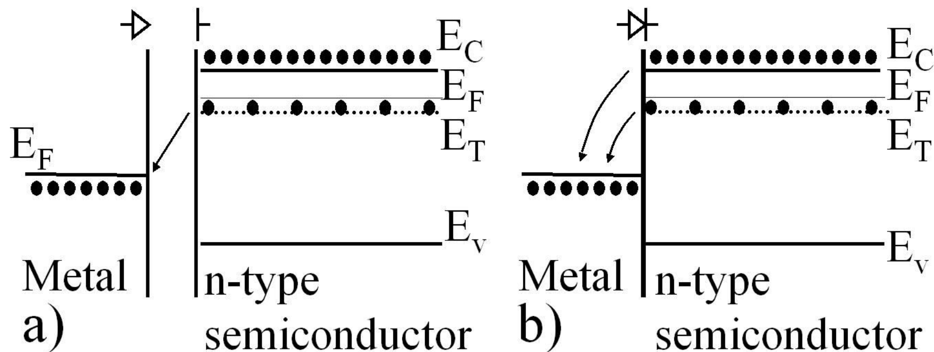

Fig. 3. Formation of a Schottky contact. a) Situation if there is no contact between the metal and the n-type semiconductor. b) Hypothetical situation if the materials would be brought suddenly into contact. No surface states that might pin the E_F are assumed. For clarity, any possible hole concentration is neglected.

The electrons deplete the region close to the metal contact, causing band bending in the semiconductor. When thermodynamic equilibrium is achieved, E_F is the same in the

semiconductor and the metal and the depletion region is formed, as shown in Fig. 4, with a certain thickness d_0, with a layer of positive ions N_{ion} (open circles with a plus sign inside). It is important to note the following: in Fig. 3 a) $E_T < E_F$ and the trap state tends to be full of electrons, but this situation changes in the depletion region when the Schottky contact has been made (Fig. 4). Due to band bending, $E_T > E_F$ in this region, and the trap tends to be empty of electrons. This relative change between E_T and E_F will have further consequences when defining a majority and a minority trap. This will be explained in more detail in Section 2.5.

It is assumed that there are no free carriers in the depletion region (this is known as the *depletion approximation*). Also a layer of electrons is formed on the metal side. The position of the layer of positive ions and of electrons should not be regarded as a function of energy, they are drawn just for descriptive purposes. The symbols of the electrons and ions will not be shown in the following images, nor the labels "metal", "n-type semiconductor" and V_{bi}.

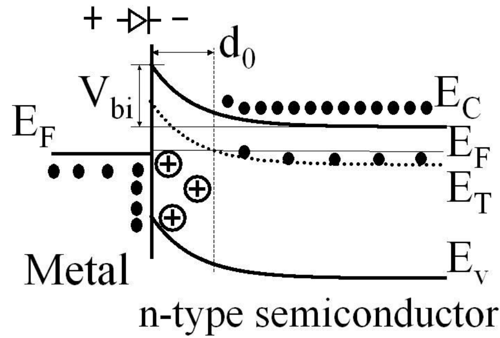

Fig. 4. Schottky contact in thermal equilibrium. There is a layer of electrons in the metal side, and a layer of positive ions in the n-type material. The depletion region in the n-type material has a thickness d_0.

According to the thermionic emission-diffusion theory[23], the current through a Schottky diode is expressed by equation

$$I = I_S\,(exp(qV/nkT) - 1), \tag{9}$$

where I_S is the diffusion current, q the charge of the electron, V the voltage across the Schottky diode according to the polarization shown in Fig. 4, k the Boltzmann constant, T the absolute temperature and n the ideality factor. I_S is a temperature dependent variable, and depends on V_{bi} according to

$$I_S = A^{**}T^2 \exp(-q\, V_{bi}/kT), \quad (10)$$

where A^{**} is the Richardson constant, a parameter depending on the effective mass of the carriers.

Usually, one plots and linearly fits the natural logarithm of I *vs.* V of Eq. 9. The constant term yields I_S, and the slope n. The parameter n is important, as it usually has a value between 1 and 2: the closer the value is to one the more the transport process is caused by the thermionic emission, and values closer to two mean diffusion is the governing transport mechanism. Values out of this range are usually attributed to low crystal quality, an interfacial layer or surface states between the semiconductor and the metal. Particularly at low temperatures, this can also be attributed to the so-called T_0 effect, which empirically states that n depends on T as

$$n = n_0 + T_0/T. \quad (11)$$

The capacitance for a Schottky contact on homogenously doped semiconductor can be expressed by the same expression as for any planar capacitor[23]

$$C = \varepsilon A/d, \quad (12)$$

where ε is the dielectric permittivity of the semiconductor, A the area of the Schottky contact and d the depletion region thickness. d is related to the built-in voltage V_{bi}, the voltage V and the total charge in the depletion region ρ (in the case of Fig. 4, $\rho = qN_{ion}$) by

$$d = (2\varepsilon(V_{bi} - V)/\rho)^{1/2}. \quad (13)$$

Combining Eqs. 12 and 13, one obtains

$$C = A\, (q\varepsilon/2)^{1/2} (\rho/(V_{bi} - V))^{1/2}. \quad (14)$$

A plot of $1/C^2$ *vs* V yields a straight line. A linear fit provides ρ and V_{bi} from the constant term and the slope, respectively.

2.4 Deep level in the depletion region of a Schottky contact

Deep levels are everywhere in the semiconductor. DLTS technique studies only those levels that are in a variable depletion region. Thus, in this Section, the deep level behavior in the variable depletion region of a Schottky contact will be described.

The analysis is done considering a Schottky contact. This is because the research was done using only Schottky contacts. Another reason is that in the literature the explanations are based on p-n junctions[20,24,25]. This discussion is divided into two parts: in Subsection 2.4.1 one deep level with an activation energy E_T smaller, but close to the Fermi level E_F is considered, and the analysis is performed for the reverse-biased diode as well as for zero bias. In the depletion region of a Schottky contact is formed, E_T gets over E_F, due to band bending. In Subsection 2.4.2, the deep level has an energy much smaller than E_F, and the analysis is done for zero-bias and forward bias. For simplicity, a n-type non-degenerate semiconductor ($N_C \gg n \gg p$) is assumed (N_C is the effective density of states in the conduction band), and thus, any possible hole distribution is neglected for the first part. In the second part, this assumption will be softened. The n-type doping is assumed to be constant and homogenous. It is also assumed that there are no surface states in the semiconductor that might pin the Fermi level.

2.4.1 Majority carrier trap

For non-degenerate n-type semiconductors in a steady state, the consequence of the assumption $N_C \gg n \gg p$ on Eq. 8 is

$$n_T = c_n n/(c_n n+e_n)\, N_T, \tag{15}$$

if the hole population is neglected. On the other hand, electrons are fermions, and they follow the Fermi-Dirac statistics in thermal equilibrium

$$n_T/ N_T \;\; = (1 + (g_1) \exp ((E_T - E_F)/kT))^{-1}. \tag{16}$$

where g_1 is the degeneracy factor. Combining Eqs. 15 and 16, one obtains

$$e_n/(nc_n) = (g_1) \exp((E_T - E_F)/kT). \quad (17)$$

For simplicity, $g_1=1$ is assumed in the following. From Eq. 17 one realizes that if $E_T > E_F$ then $e_n > nc_n$ and the deep level tends to be empty of electrons. Similarly, if $E_T < E_F$ then $e_n < nc_n$ and the deep level tends to be full of electrons. D. V. Lang originally defined an *electron trap* as one empty of electrons, *i.e.*, capable of capturing electrons[20]. Because the electrons are the majority carriers in our analysis, this trap can be said to be a majority trap. Likewise, a *hole trap* is one full of electrons, *i.e.*, capable of capturing holes. In the case of n-type semiconductor, it is also known as a minority trap. Due to this definition, the electron traps tend to be in the upper part of the band gap, and the hole traps in the bottom part. A more precise way to state this is, as seen from Eq. 17, that the electron traps tend to have a larger energy than the Fermi level, and reciprocally, the hole traps have smaller energy than the Fermi level. This is the reason why the following analysis is separated in two depending on the trap energy: whether it is larger or smaller than the Fermi level. Of course, the capture cross sections σ_n and σ_p also play a role in the definition of the electron and hole traps.

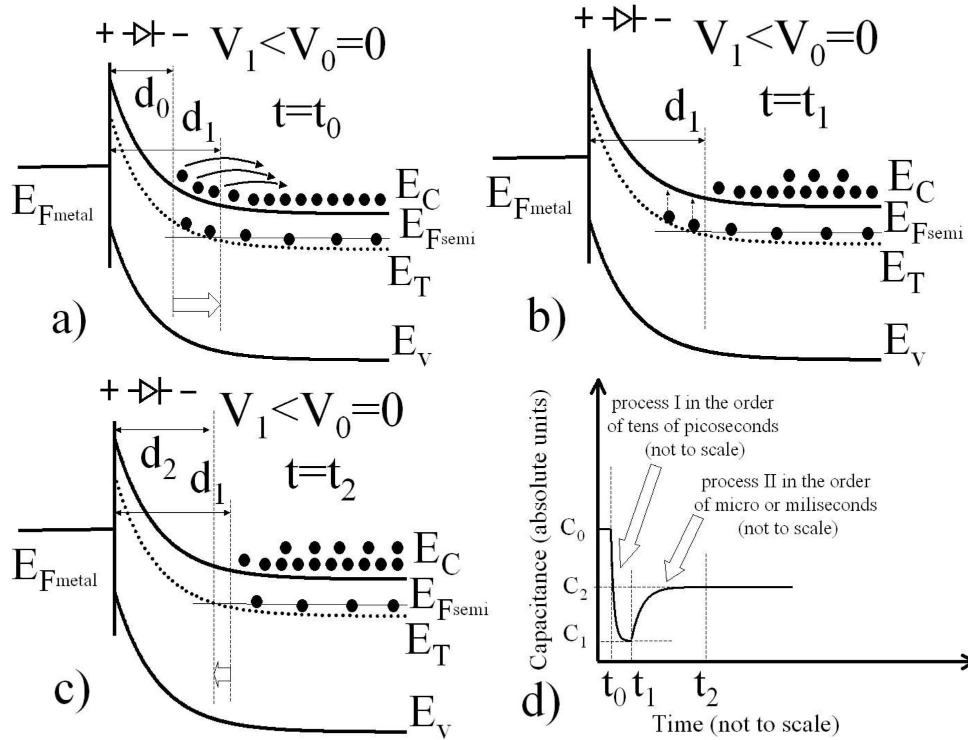

Fig. 5. Evolution of carrier distribution in a Schottky contact when it is reverse-biased. The process is described in the text.

At zero bias $V_0=0$ the Schottky contact has a capacitance of $C_0 = \varepsilon A/d_0$. Assuming that at some time t_0 the contact is reverse-biased to $V_1<V_0=0$, the free carriers are swept away from the contact region by the external potential, and their response time is in the scale of the dielectric relaxation time (ε/σ), which is a quantity in the order of picoseconds. The depletion region widens to a new thickness d_1 (open arrow in Fig. 5 a)) which can be calculated from Eq. 13. During this time $t_0 < t < t_1$, the total net charge increases in the depletion region, and the capacitance changes to a new value of $C_1 = \varepsilon A/d_1 < C_0$. After biasing the situation is as shown in Fig. 5 b). This is also process I shown in Fig. 5 d). During this period of time very few electrons are emitted from the deep level to the conduction band, as the respective time constants are in the order of micro or milliseconds. The emission times are the inverse of the emission rates, and the values that have been found experimentally are in these orders of magnitude. During this emission period $t_1 < t < t_2$, the electrons are thermally excited to the conduction band and then swept away. The depletion region shrinks to the value d_2, and the junction arrives into the state as shown in Fig. 5 c). According to Eq. 12, the capacitance increases to a new value $C_2 = \varepsilon A/d_2$. This process II is also shown in Fig. 5 d). The shrinking of the depletion region width to d_2 can be understood in two ways. The first one is done by analyzing Eq. 13. The total net charge ρ in the new depletion region d_1 increases as the electrons are emitted to the conduction band and then swept away. According to Eq. 13, d diminishes and, following Eq. 14, C increases.

A second way of visualizing this in a more clear way is using Eq. 7. During the period of time $t_1 < t < t_2$, the only process happening in the depletion region is emission of electrons to the conduction band, because the electrons are immediately swept away once they are in the conduction band and thus, they cannot be re-captured. And as the hole contribution has been neglected, Eq. 7 becomes

$$n_T(t) = n_T(0) \exp(-t/\tau_e) \tag{18}$$

In this case $\tau_e = e_n^{-1}$. Using Eqs. 13, 14 and 18, and the fact that in the depletion region $\rho = N_{ion} - n_T$, one gets

$$C = C_2 (1 - n_T(t)/ n_T(0))^{½}. \tag{19}$$

The final result, for $t_1 < t < t_2$, is

$$C = C_2 + (C_1 - C_2) \exp(-(\Delta t)/\tau_e) \tag{20}$$

where $\Delta t = t - t_1$. This explains the exponential dependence shown in Fig. 5 d). It is this exponential transient which is one of the basic ideas for the DLTS measurements, as will be shown in Section 2.4.

So far, it has been explained what happens in the depletion region with a deep level when a Schottky contact is reverse-biased. Now, it will be analysed what happens when the voltage is increased to a value $V_2 \leq 0$, which is still negative, but smaller than V_1 in absolute value. For simplicity, we assume $V_2 = V_0 = 0$, but the same analysis holds for whatever V_2 with $V_1 < V_2 < V_0$. When voltage is brought back to zero, at some time $t = t_3$, the depletion region recovers its original value d_0, and the electrons move fast (Fig. 6 b)) into the former depletion region between d_0 and d_2. Again, during a period of time $t_3 < t < t_4$, in the order of picoseconds (Fig. 6 c)), they get into the conduction band. This causes an increase in capacitance, to a value bigger than C_0 (process III in Fig. 6 f)). This can be seen from Eq. 14, as the total net charge in the depletion region is bigger than in Fig. 4: the deep levels have not captured electrons, yet. The deep levels capture electrons in a period of time $t_4 < t < t_5$ in the order of micro or milliseconds (Fig. 6 d)). This reduces the total net charge in the depletion region to the original value shown in Fig. 4, causing the capacitance to decrease back to C_0 (process IV in Fig. 6 f)). And finally, at time t_5 (Fig. 6 e)) we arrive to the original situation shown in Fig. 4.

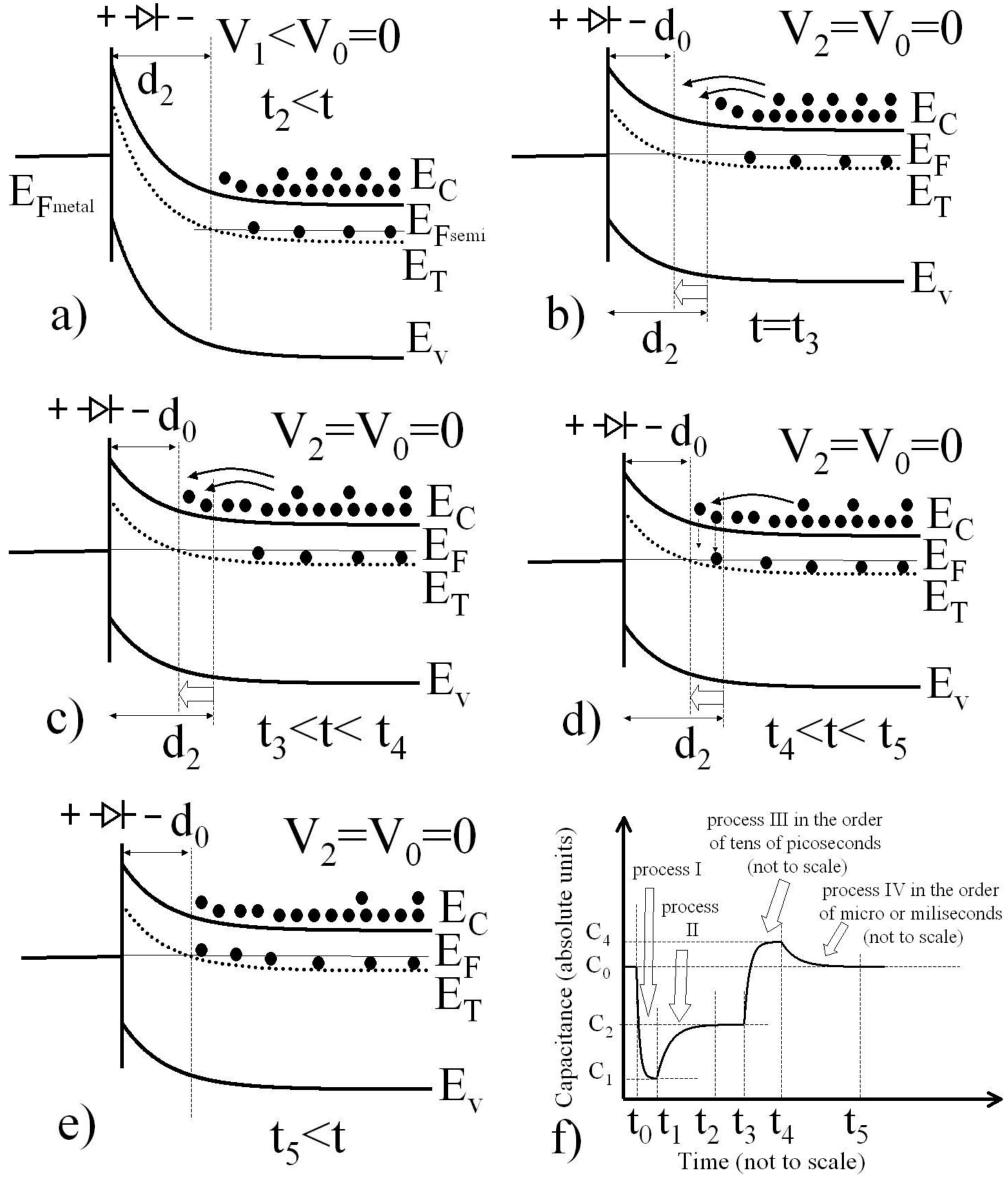

Fig. 6. Evolution of carrier distribution in a zero bias Schottky contact after being reverse-biased. Fig. 6 a) is the former Fig. 5 d). The process is described in the text.

The evolution during process IV can be understood using Eq. 7. In this case, the deep levels are empty *($n_T(t_4) = 0$),* and the process consists only of the capture of electrons from the conduction band. Eq. 7 becomes

$$n_T(t) = c_n n/(c_n n) N_T(1- \exp(-t/\tau_c)) = N_T(1- \exp(-t/\tau_c)), \qquad (21)$$

where $\tau_c = (c_n n)^{-1}$. Following a similar process as formerly described for process II, one can write the evolution of the capacitance as (for $t_4 < t < t_5$):

$$C = C_0 + (C_4 - C_0)(\exp(-t/\tau_c)), \qquad (22)$$

which explains the shape of the capacitance curve in process IV in Fig. 6 f). So far, we have described the case of an electron trap acting as a majority carrier trap. Next, a minority carrier trap is considered.

2.4.2 Minority carrier trap

It is usually said that Schottky contacts are useful only to study majority carrier properties, as they are considered to be only majority carrier devices, *i.e.,* the presence and effect of the minority carriers is neglected. This is not totally correct, as several studies have shown[26].

In those studies it has been found that minority carriers can also be trapped by minority-carrier traps in Schottky contacts during forward bias. This is due to the minority carrier quasi-Fermi level adjustment, in such a way, that the minority carrier traps are emptied. In those cases, it is necessary that the semiconductor has a very low doping, in the order of 10^{13} - 10^{14} cm^{-3}, and the forward bias is not large (~1-2 V). A similar analysis can be done as was done for the majority carrier case. Because the experimental results did not contain minority carrier traps the analysis of the minority carrier trap case will be cursory. The important fact is that the minority carrier deep levels show a capacitance transient, which is inverse compared to the majority carrier case, as shown in Fig. 7.

Briefly, process Ib corresponds to an increase in the capacitance due to forward biasing the Schottky contact. Both majority and minority carriers get into the depletion region. Both carriers flow and some minority carriers are captured by the trap level. Afterwards, when the bias of the Schottky contact is brought back to zero, a sudden decrease in capacitance occurs, because the majority carriers are swept away while the trapped minority carriers stay in the region. This is depicted as process IIb. Both processes happen in the order of picoseconds. Finally, minority carrier traps emit their carriers and cause an exponential decay in the capacitance, which is process IIIb.

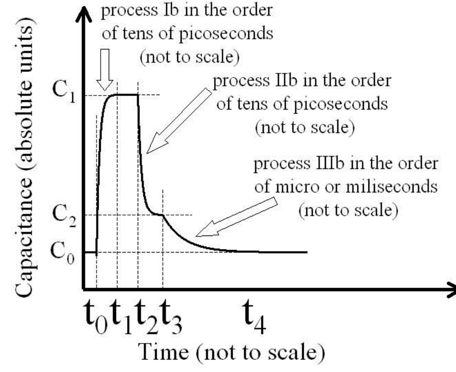

Fig. 7. Evolution of the capacitance transient for a minority carrier trap. At time $t = t_0$*, the Schottky diode is forward biased, increasing the capacitance. A constant value is obtained at* $t = t_1$*. The Schottky diode is zero biased at* $t = t_2$*. First, the capacitance rapidly decreases, and after some time* t_3*, a capacitance transient is seen. This is due to the minority carriers emitted from their trap charges.*

In a similar way as it was done for the electron trap, it is possible to find that the capacitance evolves with t during process IIIb (for $t_3 < t$) as

$$C = C_0 + (C_2 - C_0)(e^{-(\Delta' t)/\tau}), \tag{23}$$

where $\Delta' t = t - t_3$. For this case $\tau = e_p^{-1}$.

Measuring the evolution of the capacitance as a function of t yields the emission rates of the deep levels (Eqs. 22 and 23).

2.5 Principles of DLTS

D. V. Lang realized that the change in capacitance, shown in Figs. 6 and 7 as processes II and IIIb, respectively, could provide the sign of the carrier that was emitted. For process II the change in capacitance is a positive one, while in process IIIb it is a negative one. Next, it is shown that the emission process is a function of temperature. A non-degenerate n-type semiconductor, $p \ll n \ll N_C$, where N_C is the equivalent density of states in the conduction band, is considered. It is also assumed that E_F is far enough from the conduction band, so that the electrons follow a Maxwell-Boltzmann distribution

$$n = N_C\,(g_1) exp\,(-(E_C - E_F)/kT). \tag{24}$$

The principle of detailed balance states that in thermodynamic equilibrium two processes, one of which is the inverse one of the other, should have the same probability to happen. Thus, in a semiconductor in thermodynamic equilibrium, $e_n = n\, c_n$ and $e_p = p\, c_p$. It is assumed that this is true also in non-equilibrium, for example, when the semiconductor is in forward or reverse bias. This is not necessarily true, but it is usually a valid approximation, and it is one of the foundations of the DLTS analysis. In this case, combining Eqs. 24 and 17 yields

$$e_n = c_n\, N_C\, (g_1) exp((E_T - E_C)/kT). \qquad (25)$$

It is known[23] that $N_C = 2(2\pi m^* kT/h^2)^{3/2}$ and $<v_{th}>_n = (3kT/m_n^*)^{1/2}$, where m_n^* is the effective mass of electrons, h is the Planck constant and k is the Boltzmann constant. Using Eq. 4, Eq. 25 can be rewritten as

$$e_n(T) = \gamma T^2\, \sigma\, exp((E_T - E_C)/kT), \qquad (26)$$

where $\gamma = 2 * 3^{1/2} (2\pi)^{3/2} k^2 m_n^* h^{-3} g_1^{-1}$ is a constant. In general, Eq. 26 is the most used expression for e_n, but some other corrections exist, as the case when σ is temperature dependent. Those cases will not be addressed here and can be found in specialized literature[25]. Similar results can be obtained in the case of holes.

Before DLTS was proposed, the usual process to study deep levels was to analyse the capacitance transient, due to some voltage pulse, to get the emission rate, and afterwards, the deep level energy. This was done at some fixed temperature and was very time consuming, as a very detailed measurement of the capacitance transient was needed.

D. V. Lang reasoned in the following way: monitoring the capacitance change yields the emission rates. The emission rates are functions of temperature (Eq. 26). Then, instead of monitoring carefully some capacitance transient at a fixed temperature, it is better to monitor the change of the capacitance at two fixed times as a function of temperature. The biggest change in capacitance would happen when the monitoring time is in the same order as the time rate of the capacitance transient. This is shown in Fig. 8. In Fig. 8 a) several transients of a minority carrier trap at different temperatures are shown. The capacitance C_0 and C_1 are measured at times t_0 and t_1 (the difference $t_1 - t_0$ is what is known as *rate window* in DLTS "language"). In Fig. 8 b), the plot of $\Delta C = C_0 - C_1$ as a function of temperature is shown. It

forms an upward peak, which has a maximum value changing as a function of t_0 and t_1, as will be shown below.

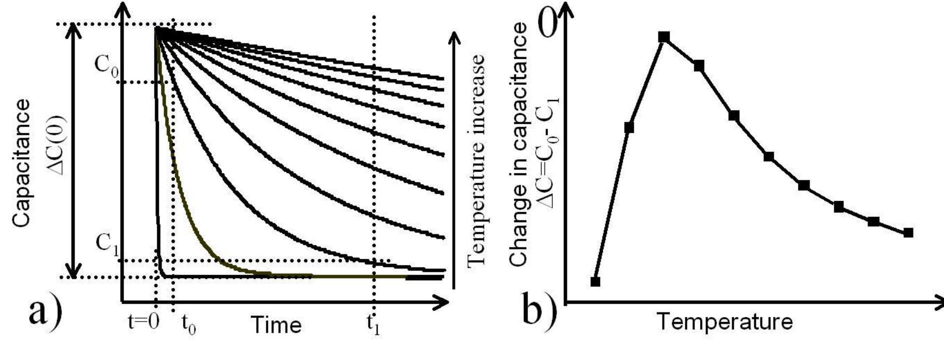

Fig. 8 a) Capacitance transients for a minority carrier trap at several temperatures. Capacitances C_0 and C_1 are measured at times t_0 and t_1, respectively, for each temperature. $\Delta C(0)$ is explained in the text. b) Change of the measured capacitances $\Delta C = C_0 - C_1$ plotted as a function of temperature.

D. V. Lang proposed the following function

$$S(T) = [C(t_0)- C(t_1)]/\Delta C(0) = [C_0 - C_1]/\Delta C(0), \tag{27}$$

where $\Delta C(0)$ is the change in capacitance between the initial state (the forward bias has been removed but the carriers have not yet been captured by the traps) and the final state (after a time long enough has passed, and the capacitance is back to constant). It is equivalent to the change $C_0 - C_2$ in Fig. 7. $S(T)$ turns out to be the signal in Fig. 8 b), but normalized with respect to $\Delta C(0)$. Writing Eq. 27 in terms of the exponentials yields

$$S(T) =[\exp(-t_0/\tau)] -[\exp(-t_1/\tau)], \tag{28}$$

where τ is the inverse of the emission rate $\tau = e^{-1}$. In order to determine the value of τ_{max} for which $S(T)$ has the largest absolute value, the derivative of Eq. 28 is calculated and set to zero. One obtains

$$\tau_{max} = (t_0 - t_1)\, [\ln (t_0 /t_1)]^{-1}. \tag{29}$$

Thus, at some values t_0 and t_1 the curve shown in Fig. 8 b) (which is a DLTS scan) will present a maximum or a minimum at some temperature T_{max}. As τ_{max} is related with the

emission, one obtains a relation of the emission rate of the trap with temperature. Making several measurements varying t_0 and t_1, one obtains a set of data between the emission rate and temperature. This set of data can be used to obtain the deep level energy E_T, capture cross section σ and the density of deep levels N_T in the following way. One can write Eq. 26 in terms of logarithms as

$$ln(e_n(T)/T^2) = ln(\gamma\sigma) + (E_T - E_C)/kT. \quad (30)$$

Hence, using the collected data set, one can plot the points calculated from the left-hand side of Eq. 30 as a function of $1/T$ (known as the *Arrhenius plot*). Linear fitting will yield the capture cross section σ and the deep level energy E_T. The trap concentration can be obtained *via* Eq. 15. This same analysis can be done for a majority carrier trap. In this case, the curve in Fig. 8 b) will have a negative sign.

Sometimes unrealistic capture cross sections are found, for example, they span over a wide range of orders, or they are geometrically senseless, *i.e.,* much bigger or smaller than a geometrical factor would suggest. In this case it is important to use the compensation law, also known as the Meyer-Neldel rule[27]. This law appears in several branches of physics, such as solid-state diffusion in crystals[28], thermally stimulated processes in polymers[29], dielectric relaxation and conduction in polymers[30] and electronic conduction in amorphous semiconductors[31].

In general terms, this rule states that if some physical quantity Γ obeys the equation

$$\Gamma = \Gamma_o \, exp\,(-E/kT) \quad (31)$$

then Γ_o and E follow the equation

$$ln\,\Gamma_o = a + bE \quad (32)$$

where a and b are constants, E is known as an "*activation energy"* and k is the Boltzmann constant.

The Meyer-Neldel rule also applies for deep levels. It states that it is not the activation energy of the deep levels which should be considered, but the Gibbs free energy $\Delta G = -\Delta H + T\Delta S$. In this case, Eq. (30) should be rewritten as:

$$ln(e_n(T)/T^2) = ln(\gamma\sigma) - (\Delta H - T\Delta S)/kT. \quad (33)$$

where ΔH is the enthalpy change and ΔS is the entropy change. A Meyer-Neldel plot is done, which yields the correct deep level parameters. Further details can be found in the literature[32].

Sometimes, the leakage current distorts the results. The common practice is to neglect the leakage current if it is smaller than 10 µA. However, it has been analyzed that even lower leakage current can affect the DLTS measurement[33]. In this case, free carriers are introduced into the depletion region during reverse bias. They are captured by the deep levels, giving rise to errors in measured capacitance. The best way to proceed in this case is to measure the leakage current and the DLTS spectrum at the same time, and then, *via* simulations, obtain the corrected DLTS parameters[33].

The usual setup for a DLTS measurement consists of a variable temperature cryostat, one or two pulse generators (in the order of picoseconds) capable of making rapid changes in the diode bias and a sensitive capacitance measurement apparatus with a good transient response. When it was first proposed, a dual-gated signal integrator was used to integrate the signals, providing a more accurate measurement of the difference in capacitance. As electronics has developed and more accurate capacitance measurement apparatus have appeared, the use of the dual-gate integrator has become obsolete.

Fig. 9 shows the usual procedure. Fig. 9 a) corresponds to majority carrier traps and Fig. 9 b) to minority carrier traps. The sample is reverse biased at some voltage V_R. The voltage is rapidly increased and decreased in periodic pulses. The length of the pulses might be micro or miliseconds. They are the former processes I and III of Fig. 5 d) and Fig. 6 f), and processes Ib and IIb of Fig. 7. During the pulse the capacitance increases. After the pulse the capacitance rapidly decreases and then the capacitance transients due to the refilling of the deep levels are seen (they are the former processes II of Fig. 5 d) and Fig. 6 f) and process IIIb of Fig. 7). The analysis shown above can be performed on the transients to obtain the deep level parameters.

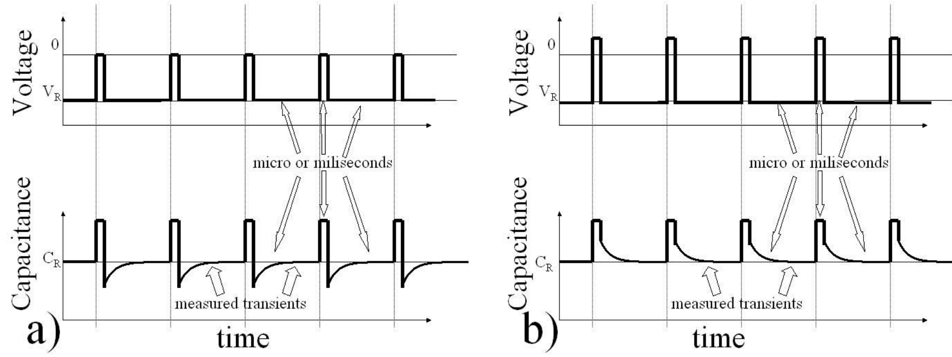

Fig. 9. Periodic voltage pulses and the respective capacitance changes. The curves correspond to a) majority carriers and b) minority carriers.

Several variants of the DLTS technique have been suggested during the last 30 years. For example: double correlation DLTS (DDLTS) yields deep level profiles and excludes the field dependence of the capture cross section and contact effects[34]. It is based on two pulses instead of one. In this way, the trap concentration profile can be obtained by varying the rate windows, the pulse amplitudes and the reverse bias.

Another variation is constant capacitance DLTS (CCDLTS)[35]. In this technique, the applied voltage is varied during the temperature scan to keep the capacitance constant, and thus, also the depletion width constant. It is this time-varying voltage that provides the trap information, permitting more accurate measurements of defect profiles at high trap densities; it has shown to be very good for trap concentration profiling, especially when combined with DDLTS.

A third variation of DLTS is optical DLTS (ODLTS)[36]. In this technique, light is used to excite the carriers, instead of the electrical filling pulses. In one version of ODLTS, variable-energy light replaces the temperature scan. In the analysis of ODLTS data, the emission rate e_n must be replaced by $e_n + e_n^0$, where $e_n^0 = \sigma_n^0 \phi$ is the optical electron emission rate, ϕ is the photon flux density and σ_n^0 is the optical electron capture cross section. A major advantage of ODLTS is that minority carriers can be easily generated *via* optical stimulation. ODLTS has been shown to be useful for investigation of deep levels in semiconductors with wide band gaps.

Deep level transient Fourier spectroscopy (DLTFS) and Laplace DLTS (LDLTS)[37] use Fourier and Laplace transform, respectively, to manipulate data. The determination of

Fourier and Laplace coefficients is equivalent to making several DLTS scans with different rate windows, i.e., one saves time: instead of making several scans, one needs to make a single one and then obtain the Fourier and Laplace coefficients. This improves the results, because peak amplitude is not dependent on temperature anymore. It also gives better noise suppression.

Isothermal Transient Spectroscopy (ITS)[38] uses the same principles, but with a different approach. In DLTS the scanning is done over the temperature at some fixed rate window. In ITS, the temperature is fixed at some value, and it is the rate window which is scanned. This technique is helpful in the case when the capture cross section is very temperature dependent. Usually it is necessary to do a DLTS scan, first in order to know the temperature position of the peaks.

Positron DLTS (PDLTS) uses positrons as probes[39]. It is very useful to know if the defects have vacancies attached to their microstructure, and to get information about the internal electric field in the semiconductor.

All these techniques are improvements on the acquisition of deep level parameters, such as activation energy, density, capture cross section, profiles, etc… But still, sometimes it is difficult to separate deep level signals having very similar activation energies.

Chapter 3

Use of inductors in DLTS

In this work, the use of inductors to improve the data acquisition by DLTS has been researched. The general electrical model for a Schottky contact is shown in Fig. 10.

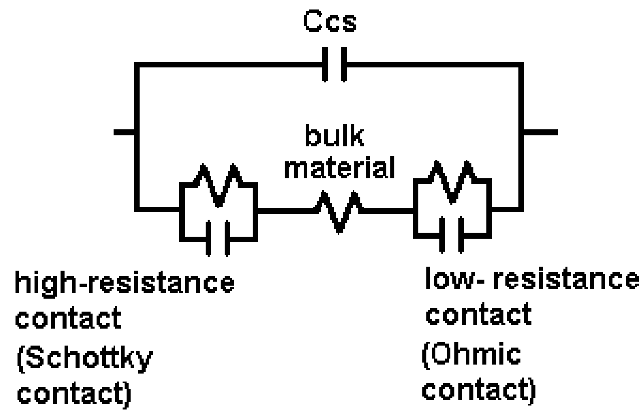

Fig. 10. Equivalent circuit of a total (two-contact) Schottky diode. C_{CS} is the parasitic capacitance of the package.

For unpackaged DLTS samples C_{CS} is zero. In general, both the bulk material and the ohmic contact contribute negligibly to the resistance and capacitance of the sample, *i.e.*, they can be discarded. Thus, the model comprises a parallel resistance and capacitance, as shown in Fig. 11 b).

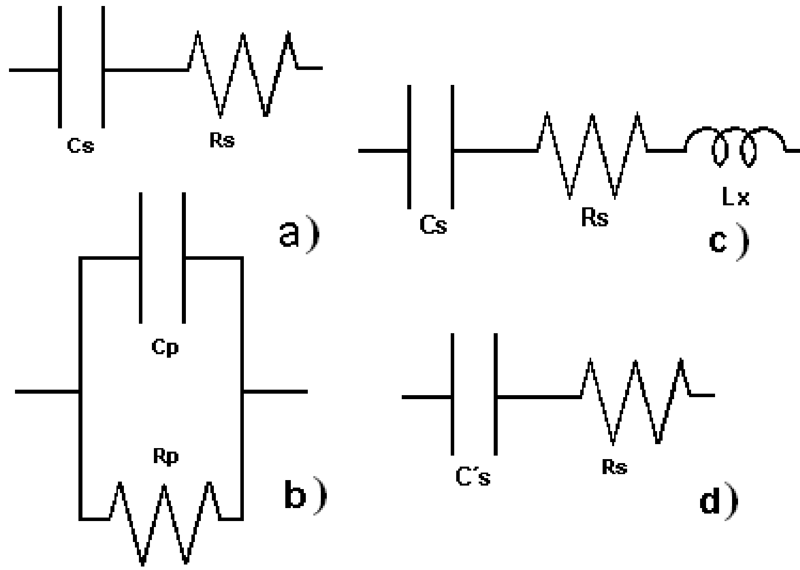

Fig. 11. a) Series equivalent circuit of the Schottky diode, b) parallel equivalent circuit of the Schottky diode, as seen by the capacitance meter, c) series equivalent circuit of the Schottky diode with an inductor in series, and d) series equivalent circuit of the Schottky diode with a capacitance which accounts for both the Schottky capacitance and the inductance.

The series model of Fig. 11 a) is preferred, because this makes it possible to regard the capacitance and resistance measured in DLTS directly as those of the Schottky contact[40]. It has been shown that the series capacitance C_S and the series resistance R_S (Fig. 11 a)) are related to the parallel capacitance C_P and parallel resistance R_P through[41]

$$C_P = C_S /(1+Q^2) \quad \text{and} \tag{34}$$

$$R_P = R_S (1+1/Q^2), \tag{35}$$

where $Q = R_S C_S w$ is the quality factor of the series circuit (Fig. 11 a)) and w is the frequency of the drive signal delivered by the capacitance meter.

The capacitance meter measures the capacitance of the parallel circuit (Fig. 11 b)). Usually, it is supposed that the Schottky contact only shows a capacitive nature[11], *i.e.*, $R_S = 0$. Under this assumption $Q = 0$ and then $C_P = C_S$. Broniatowski *et. al* have suggested that the effect of a properly chosen inductance in series with the Schottky contact might increase the signal-to-noise ratio[41]. In publication I, the effect of an inductance in series with a Schottky contact was researched experimentally. It was found that signal-to-noise ratio does not increase,

actually it becomes smaller. But the benefit is that the separation of the signals that are too close to each other becomes possible.

Also another application for inductors was found (publication II). If an inductance L_X is attached in series with a Schottky contact (Fig. 11 c)), the resulting series circuit is equivalent to the original series model of a Schottky contact (Fig. 11 a)), if one assumes a new series capacitance C'_S (Fig. 11 d)) given by

$$C'_S = C_S /(1-w^2 L_X C_S). \tag{36}$$

Introducing C'_S of Eq. 36 into Eq. 34, one gets a measured parallel capacitance C'_P $(L_X \neq 0)$

$$C'_P = C_S (1-w^2 L_X C_S)/((1-w^2 L_X C_S)^2 + (R_S C_S w)^2). \tag{37}$$

Using Eq. 37 it is possible to obtain the correct series capacitance and series resistance of the Schottky diode. Namely, performing two separate measurements, one DLTS scan without an inductor to obtain C_P, and another one with a series inductor L_X attached in the circuit to yield C'_P. Solving Eq. 37 for C_S and R_S as a function of C_P and C'_P yields

$$C_S = (C_P - C'_P +2 w^2 L_X C_P C'_P)/((w^2 L_X C_P)\times (1+w^2 L_X C'_P)) \text{ and} \tag{38}$$

$$R_S=((C_S- C_P)/C_P)^{1/2}/(w C_S). \tag{39}$$

This idea was tested using a gold Schottky contact deposited on a 2 µm thick *n*-type $Al_{0.4}Ga_{0.6}As$: Si layer grown by Molecular Beam Epitaxy (MBE). An annealed ohmic contact (5 nm Ni / 5 nm Au / 30 nm Ge / 100 nm Au) was deposited on the back of the n+ substrate. Four inductors with L_X = 3.413, 4.543, 6.665 and 8.51 mH in series with the sample were tested to get a set of C_S's and R_S's. They are shown in Fig. 12, as a function of temperature.

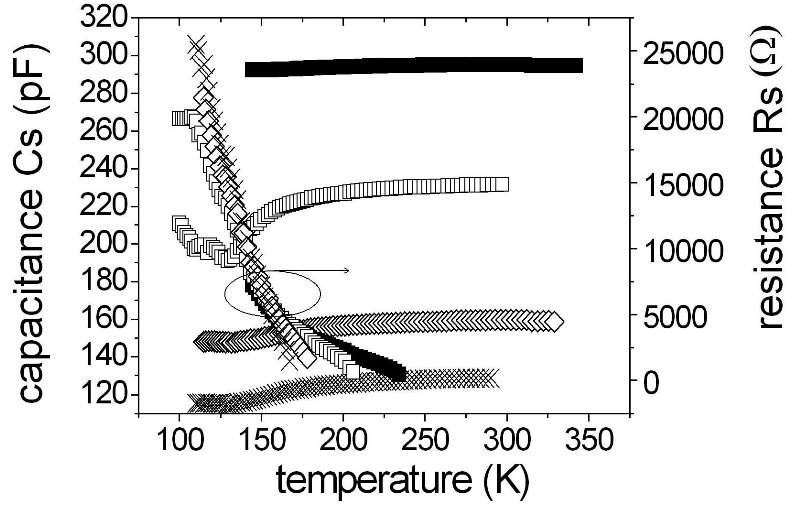

Fig. 12. Series resistance and series capacitance measured for n-type $Al_{0.4}Ga_{0.6}As$: Si epitaxial layer on a n-type GaAs (100) substrate, with a pulse width of 100 ms and a period width of 1 s, obtained by applying Eqs.35 and 36. The graphics correspond to the following inductances: 3.413 mH (■),4.543 mH (□),6.665 mH (◊) and 8.51 mH (×).

Several conclusions can be obtained from these curves. First of all, R_S behaves as expected in a semiconductor, *i.e.*, it increases as the temperature decreases. It is independent of the applied inductance, L_X (slight variations in R_S at high temperature are attributable to an inductance effect from the ohmic contact[42]) as predicted by Eq. 39. But mainly, R_S is far from being zero, particularly at low temperatures. This has a deep impact on data obtained from the DLTS scan, as the quality factor becomes non-negligible (Q > 1) as the temperature decreases (Fig. 13).

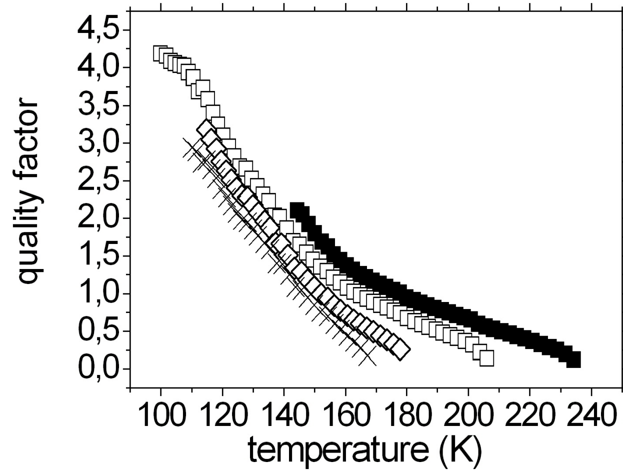

Fig. 13. Quality factor Q obtained for $Al_{0.4}Ga_{0.6}As$: Si with a pulse width of 100 ms and a period width of 1s. It appears that $Q \neq 0$ over a large temperature range, in sharp contrast to what is often assumed. The graphics correspond to the use of the following inductances: 3.413 mH (■),4.543 mH (□), 6.665 mH (◊) and 8.51 mH (×).

The parameter Q shows some interesting features: it is independent of the inductance, as expected; it increases as the temperature decreases, being bigger than 1 below 160 K, and almost 5 at 100 K. If C_S were considered to be the same as the measured C_P read from the capacitance meter and were not corrected for $Q \neq 0$, an error of an order of 25 in C_P would occur at 100 K. This error becomes less important at higher temperatures, but it might alter the DLTS parameters of the semiconductor, as at least GaInNAs[43], GaNAs[44], InP[45] and AlGaAs[46] exhibit deep levels in the range of 85 to 200 K. The density of deep levels is strongly affected by this error because it is inversely proportional to C_P during reverse bias. The activation energy of a deep level depends upon the position of the peak in temperature scale, which is distorted by the presence of high resistance.

In summary, the use of inductors in series with a Schottky contact can bring several benefits during a DLTS measurement: close peaks may be separated, yielding a more accurate activation energy of the deep levels; the real series resistance and series capacitance of the Schottky contact as a function of temperature can be calculated, and the measured DLTS curve can be corrected *via* Eqs. 34 and 35, so the correct activation energies, densities and capture cross section can be calculated.

Chapter 4

Electrical characterization of GaInAs

The first proposal of GaInAs dates back to the end of the fifties[47]. In the sixties, it was found to have superior properties to the Si-Ge alloy for temperatures below 600 ^{o}C for thermoelectric power generation[48]. This encouraged the study of its thermal and electrical properties[49]. In those times, microwave amplification by stimulation emission of radiation (MASER) was studied, and GaInAs was proposed as a suitable material to achieve wavelengths between 0.84 μm and 3.1 μm[50]: the wavelengths of GaAs and InAs, respectively.

Many interesting properties have been found in GaInAs with low In composition[51-66]: doping GaAs with isovalent In reduces the amount of dislocations and improves the epitaxial quality[51-57]. Indium incorporation also increases the concentration of carriers[52] and causes higher mobility[62], improves the fabrication of high-quality GaAs Schottky diodes using a strained layer[58], enhances the carrier lifetime and diffusion length in GaAs[59] and helps to fabricate a low-loss optical waveguide using GaInAs superlattices[61]. The first DLTS study of GaInAs with different In percentages (4.6 %, 7.7 %, 9.9%, 14 %, 21 % and 24 %) was done in the seventies on vapour phase epitaxy (VPE) grown material[67]. It was necessary to wait until the end of the eighties to find more DLTS studies with low In composition: one on p-type GaAs In doped grown by liquid encapsulated Czochralski (LEC)[64] and several ones on molecular beam epitaxy (MBE) grown material[65,66,68-73]. Very few studies can be found on bulk GaInAs grown by metal-organic vapour phase epitaxy (MOVPE) with low In composition: one with 6 % In doped with S on n+ GaAs substrate[74], and another one with 14 % In on n-type GaAs substrate[75]. It is possible to find also some DLTS studies on quantum wells (QW)[76-77] and quantum dots (QD)[78] made of MOVPE-grown GaInAs.

GaInAs is also attractive with higher In compositions, as $Ga_xIn_{1-x}As$ (x = 0.47) lattice matched to InP shows infrared sensitivity (~900 – 1600 nm), which makes it a useful material for optical communication, photodiodes, solar cells and laser diodes[79-84].

Our goal in this study was to better understand deep levels in GaInAs. As it has been described, GaInAs is a very useful material for making lasers and for other optical and electronic applications. But the laser properties can be affected by the presence of deep levels. In order to have a better understanding of how the incorporation of In into GaAs

generates deep levels, GaInAs with a low In composition has been studied. This was done with the purpose to easily compare the results with the available literature for the deep levels in GaAs. Also the effect of annealing treatment has been studied, in order to obtain information about how the deep level concentrations could be manipulated. GaInAs with a low In composition (1.4 %) was grown by MBE for publication III. This composition was confirmed by XRD. The samples were studied by *I-V*, *C-V*, DLTFS and ITS techniques[37,38]. The samples were studied after growth and also after annealing at several temperatures (625°C, 650 °C, 675 °C, 700 °C and 750 °C) for 5 min. The processing was done following typical photolithographic techniques, which might affect the surface and bulk of the material, as SiO_2 was deposited and removed in some places. Also some Si and O might have diffused into the samples, as the annealing was done while the samples were capped with SiO_2, in order to avoid any out-diffusion.

For the *I-V* and *C-V* studies, the Schottky contacts were biased from –1.5 V to 0 V. The breakdown voltage was around –1.7 V. The ideality factor decreases from a value of 1.9 for the as-grown sample to 1.5 for the sample annealed at 750 °C. In all cases it is below 2, which is usually considered satisfactory for a reliable Schottky contact. As the annealing temperature increases, the leakage current also increases, from 2.3×10^{-7} A to 1.9×10^{-6} A showing degradation in the Schottky contact. The saturation current is in all cases well below 10 μA and the deep levels are not perturbed by a large leakage current during the reverse bias. Therefore, the depletion regions are really depleted from electrons during the reverse bias. All the *I-V* curves show a correlation value well above 0.99. The *C-V* study gives a carrier concentration of 6.8×10^{17} cm^{-3}.

For the DLTFS and ITS study, the samples were reverse biased at –0.7 V. The pulse bias was 0 V. The DLTFS curves and the respective Arrhenius plots are shown in Fig. 14 a) and b), respectively.

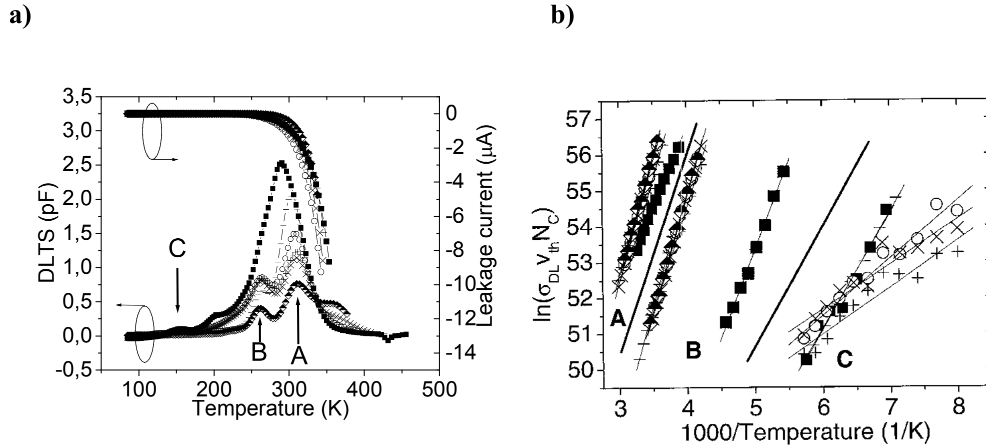

Fig. 14. a) DLTFS curves and leakage currents of Si - doped $Ga_{0.986}In_{0.014}As$ measured with a pulse width of 100 ms, a period width of 100 ms, a reverse voltage of –0.7 V, and a pulse voltage of 0 V. b) Arrhenius plot for the DLTFS measurements. N_C is the effective density of states, v_{th} is the mean thermal velocity and σ_{DL} is the capture cross section. The data points correspond to the following thermal annealing temperatures: as-grown (■), 625 ^{o}C (−), 650 ^{o}C (○), 675 ^{o}C (+), 700 ^{o}C (×), 750 ^{o}C (⬘). The annealing time was 5 min. The thick lines are used to separate the respective group of data for each deep level.

It can be seen from Fig. 14 a) that the DLTFS curve of the as-grown sample shows one major peak having remarkable broadness, and that around 265 K there is a slight shoulder. This could be due to a convolution from two trap levels. Support for this hypothesis comes from the sample annealed at 625 ^{o}C. The main peak has separated into two smaller peaks, labelled A and B, between 250 K and 350 K. It is not clear if the presence of peak B experiences any decrease from the as-grown sample to the one annealed at 625 ^{o}C, as it could be possible that only peak A decreases. Annealing at 650 ^{o}C, 675 ^{o}C and 700 ^{o}C shows that peak A decreases with increased annealing temperature, while peak B practically remains the same. Both peaks experience a decrease for annealing at 750 ^{o}C. The Arrhenius plots for the DLTFS can be seen in Fig. 14 b). The Arrhenius plot of the ITS measurements can be seen in Fig. 15.

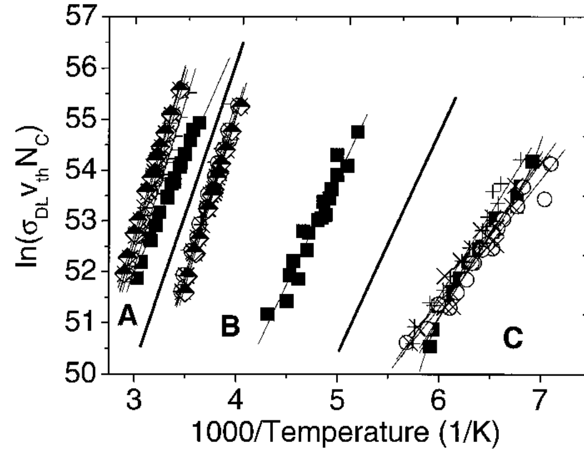

Fig. 15. Arrhenius plot for the ITS measurements of the traps A, B and C. N_C is the effective density of states, v_{th} is the mean thermal velocity and σ_{DL} is the capture cross section. The data points correspond to the following thermal annealing temperatures: as-grown (■), 625 °C (−), 650 °C (○), 675 °C (+), 700 °C (×), 750 °C (⬘). The annealing time was 5 min. The thick lines are used to separate the respective group of data for each deep level.

The DLTFS and ITS studies yield the activation energies of 0.58 eV, 0.55 eV and 0.27 eV for peaks A, B and C, respectively, in the as-grown sample. The evolution of the activation energy and density of the three traps as a function of annealing temperature can be seen in Fig. 16. The activation energy of 0.4 eV determined for the deep level A in the as-grown sample is incorrect because of overlapping of the peaks A and B. The correct value of 0.58 eV was obtained by simulation of the peaks, and it is in agreement with the values obtained from the annealed samples. Interestingly, the activation energy of the deep level C diminishes to a value around 0.15 eV after annealing at 650 °C, and it remains around this value for higher annealing temperatures.

This behavior and comparison with the literature strongly suggest that peak A is related to M5 deep centre caused by α misfit dislocations. Peak B strongly resembles deep level EL4, which is related to As-rich material and caused by point defects or point defect/impurity complexes. Because peak B has a very similar activation energy and behavior to peak A, it could also be related with dislocations. Further study is necessary to clarify this point. Peak C is attributed to deep centres EL10 and M1, and due to the invariance of the density with annealing it is presumed to be related with a point defect and/or impurity.

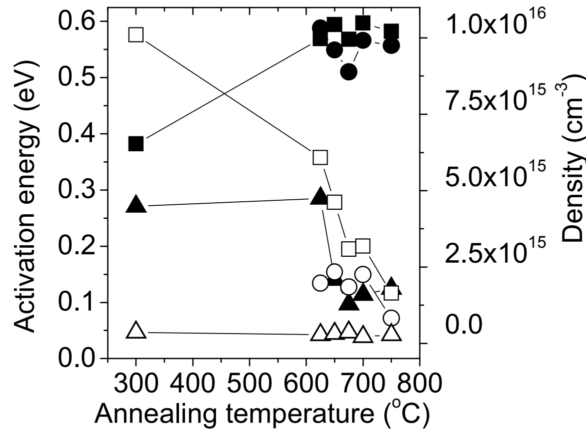

Fig. 16. Activation energy E_A for the deep levels A (■), B (●) and C(▲) and ρ_{DL} for the deep levels A (□), B (○) and C(Δ) obtained from the ITS Arrhenius plots. The as-grown sample is shown at 300 ^oC, which is the temperature for SiO_2 deposition.

The results obtained show that there are three main deep levels in GaInAs with a low In composition. The density of the deep level labeled A can be reduced with annealing treatment at 650 ^{o}C. The concentration of deep level B can be reduced at the annealing temperature of 750 ^{o}C. Deep level C seems to be unaffected by the annealing treatment.

In the future, the effect of deep levels A, B and C on laser performance should be studied. It is not easy to make DLTS on laser structures. Thin layers, inhomogeneous doping concentration profiles and different band structures are obstacles to achieve a suitable DLTS measurement, and hence, to make a reliable analysis of the results. Nevertheless, a comparison between the laser performance and the deep level structure could be made by fabricating a GaInAs layer with a similar In composition of 1.4% in the laser structure. Same growth conditions should be used in order to compare with these DLTS results. The laser structure should be annealed at similar temperatures as in this study and its performance tested, in order to indirectly infer any deep level effect and correlate it with the results of this article.

Chapter 5

Electrical characterization of GaInNAs

In 1996 Masahiko Kondow *et al.* had the idea that introducing N into GaInAs will enhance the desired lasing characteristics of GaInAs/GaAs structures[86]. Their expectations were based on the fact that adding N to GaAs decreases the lattice constant and the band gap, causing tensile strain[87]. This is a very unlikely effect, as usually the band gap is increased when the lattice constant is decreased. By using a quaternary compound, GaInNAs, the layer can be lattice-matched to GaAs substrate and have an even smaller band gap than GaInAs with similar In composition. In this way the formation of dislocations and, thus, the density of deep levels can be reduced.

In their first proposal they experimentally proved the feasibility of GaInNAs for long-wavelength-range laser diodes[86]. Later on, the application of the material for lasing has been corroborated[88-90], and it has been found useful for other applications as well, e.g., heterojunction bipolar transistors[91] and high-efficiency solar cells[92-94].

Our objective with this research was to better understand deep levels in GaInNAs. Usually QW structures of GaInNAs with quite high concentrations of In and N are needed to reach the telecommunication wavelengths. Therefore, these concentrations have also been used in the material studies. These studies do not provide insight on how a low concentration of In and N alter the deep levels in GaAs. In order to have a better understanding of how the incorporation of low amounts of In and N into GaAs generates deep levels, bulk GaInNAs with small In and N compositions has been studied. This was done with the purpose to easily compare the results with the available literature for deep levels in GaAs[95]. The effect of annealing treatment has also been studied, in order to obtain information about how the deep level properties can be manipulated. The deep level characteristics were also studied using different doping levels.

In publication V samples with low In and N compositions were studied. Although this approach is very similar to the one made by Polyakov[96] *et al.*, the results are very different. They studied a sample with 1% In and 0.35% N and similar doping (7×10^{16} cm^{-3}) to one of the samples of this thesis, and they found two deep levels. In publication V five deep levels were found. Also the behavior of these new levels following annealing at a range of temperatures is reported.

In publication V Si-doped n-type $Ga_{0.987}In_{0.013}N_{0.0043}As_{0.9957}$ lattice matched to GaAs grown by gas source molecular beam epitaxy (GSMBE) was studied. Two levels of doping were used: medium (2×10^{16} cm^{-3}) and heavy (1×10^{18} cm^{-3}). The samples were grown on a n-type GaAs (100) substrate. GaInAs single quantum wells (SQW) with a thickness of 7 nm were grown to calibrate the In composition, by comparing dynamical theory simulations with the experimental double crystal x-ray diffraction (XRD) rocking curves. The N composition was calibrated by lattice matching GaInNAs with the substrate. This was verified by XRD. Other details of the growth may be found in Ref. 97. Deep level transient Fourier spectroscopy (DLTFS) was used to study the electrical properties[37].

The thermal treatment consisted of 5 min annealing at 650 °C, 700 °C, 750 °C or 800 °C in a thermal annealing furnace under flowing nitrogen. In order to avoid out-diffusion the samples were capped with 200 nm SiO_2 deposited by plasma enhanced chemical vapor deposition at 300 °C before the thermal treatment. Figs. 17 a) and b) show DLTFS curves and the Arrhenius plots respectively for the medium-doped sample are shown.

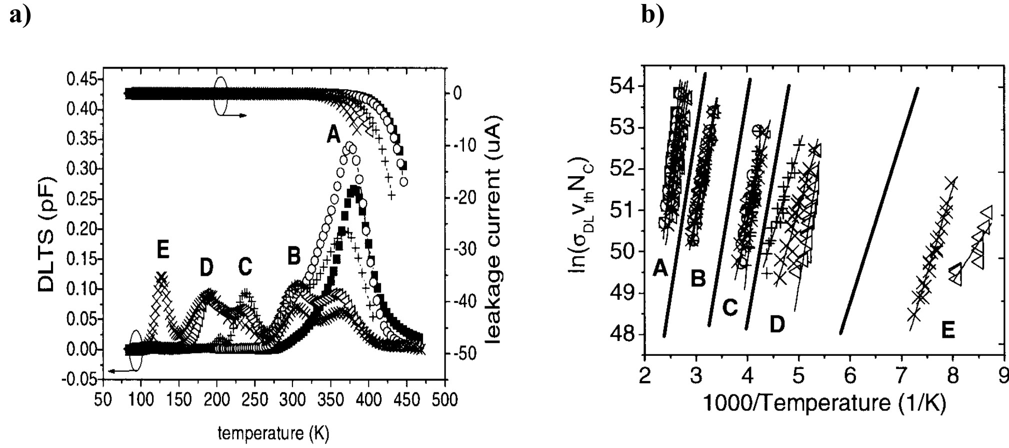

Fig. 17. a) DLTFS curves and leakage currents of the medium Si - doped $Ga_{0.987}In_{0.013}N_{0.0043}As_{0.9957}$ sample measured with a pulse width of 100 ms, a period width of 100 ms, a reverse voltage of –0.7 V, and a pulse voltage of 0 V. b) Arrhenius plot for the DLTFS measurements shown in a). N_C is the effective density of states, v_{th} is the mean thermal velocity and σ_{DL} is the capture cross section. The data points correspond to following thermal annealing temperatures: none (■), 650 °C (○), 700 °C (+), 750 °C (◁) and 800 °C (×). The annealing time was 5 min. The thick lines are used to separate the respective group of data for each deep level.

For the as grown sample, only one peak is seen (peak A) around 375 K. It shows a small shoulder around 300 K. The height of the peak A experiences a slight increase for annealing at 650 ^{o}C, and diminishes for higher annealing temperatures. The shoulder becomes more prominent after annealing at 650 ^{o}C, and it becomes a noticeable peak (peak B) after annealing at 700 ^{o}C. The peak height decreases but only a little with annealing temperature. Also a new peak appears around 250 K after annealing at 700 ^{o}C (peak C). The height of peak C diminishes only slightly at higher annealing temperatures. Peak D appears after annealing at 750 ^{o}C, and the height of this peak remains constant also after annealing at 800 ^{o}C. Finally, peak E appears when annealed at 800 ^{o}C. The Arrhenius plots in Fig. 17 b) show good linearity for the as-grown sample. The data become more and more scattered as the annealing temperature increases.

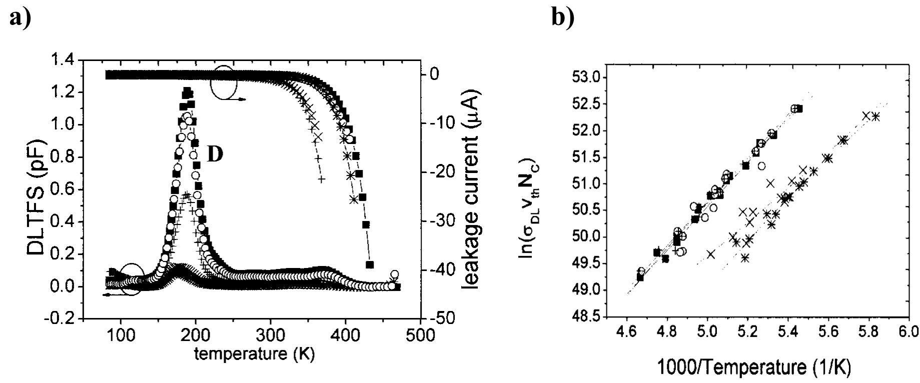

Fig. 18. a) DLTFS curves and leakage currents of the medium Si - doped $Ga_{0.987}In_{0.013}N_{0.0043}As_{0.9957}$ sample measured with a pulse width of 100 ms, a period width of 100 ms, a reverse voltage of –0.7 V, and a pulse voltage of 0 V. b) Arrhenius plot for the DLTFS measurements shown in a). N_C is the effective density of states, v_{th} is the mean thermal velocity and σ_{DL} is the capture cross section. The data points correspond to following thermal annealing temperatures: none (■), 650 ^{o}C (O), 700 ^{o}C (+), 750 ^{o}C (◁) and 800 ^{o}C (×). The annealing time was 5 min.

In Fig. 18 a) and b) DLTFS curves and the Arrhenius plots for the heavy doped sample are shown, respectively. Only peak D appears in the DLTS scan. The height of this peak decreases slightly when annealed at 650 ^{o}C, but diminishes to half of its original value when annealed at 700 ^{o}C. After annealing at 750 ^{o}C and 800 ^{o}C the height is diminished even more. The data in the Arrhenius plot (Fig. 18 b)) become more scattered as the annealing temperature increases.

In total there are at least 5 electron traps, some of which can be compared to well known deep levels in GaAs. For the medium-doped as-grown sample, the strongest signal comes from the deep level corresponding to peak A. This trap level might be related to the native arsenic antisite (As_{Ga}) labeled EL2 in GaAs[98]. Peak B is almost not affected by thermal annealing. Comparison with the study of $Ga_{0.986}In_{0.014}As$ (publication III) shows that it is not related with N and it is very likely related with the off-centre substitutional oxygen in As sites. Peak C appears only after annealing at 750 ^{o}C and is affected very little by higher annealing temperatures. Comparison with the study of $Ga_{0.986}In_{0.014}As$ (publication III) suggests that N is involved, maybe because of clustering of GaNAs and GaInAs. Peak D appears after annealing at 750 ^{o}C and is almost not affected by higher annealing temperatures. It is the only one that appears in the heavy-doped sample, where it is very sensitive to annealing. It has been reported to be intrinsic to GaAs, which suggests that N is not involved in it. It could be caused by As interstitials and antisites. The presence of N might lower the probability of the formation of these As-related defects. This peak is the only one, which appears for the heavy-doped sample. Finally, peak E is seen only after annealing at 800 ^{o}C. This level is scarcely reported in the literature. It cannot be reliably evaluated and we assume it is due to high disorder introduced to the material due to the high annealing temperature.

The characteristics of the deep levels for GaInAs and GaInNAs, and their behavior after annealing, should be valuable for researchers interested in using these materials for any optoelectronic application. Annealing at suitable conditions should be a useful tool to tailor the presence of these deep levels. These studies could be continued further, by studying how higher concentrations of In and N change the deep level characteristics. The effects of these deep levels on the device performance should be also tested, *e.g.*, similarly as was suggested in Chapter 4. Different doping levels and annealing conditions could be explored, and depending on the changes in photoluminescence, DLTS and possible relations could be found.

Chapter 6

Electrical characterization of InN

InN has not been as deeply studied as the other III-N semiconductors, due to difficulties in preparing high quality material. Despite the first mention of InN was very long time ago[99], very little research was done until the eighties. Studies of InN are closely linked with the studies of GaN. It must be remembered that GaN attracted a lot of attention when the first high-brightness commercial blue light emitting diodes (LED) based on nitride semiconductors appeared on the market. This was a little over a decade ago, and now GaN is the second most important semiconducting material after silicon, with US $1.33 billion in sales in 2002 and projected sales of US $4.55 billion for 2007[100]. Alloying GaN with In, thus forming GaInN, made it possible to extend the wavelength range of the GaN LED from ultraviolet to green.

Previously, it was assumed that the band gap of InN was a direct gap[101] with a value of about 1.9 eV. Recently, however, band gap energies smaller than 1.9 eV have been reported[102,103], namely, in the range of 0.7 – 1.0 eV. Corresponding wavelengths are compatible with the wavelengths used in optical communication. If InN of high crystalline quality could be grown, it could have a major impact on the optical communication industry in a large number of applications[104]. It could be said, that nowadays InN is in the same development phase as GaN was approximately fifteen years ago[105]: many new and exciting properties are found, maybe triggering future applications. Nevertheless, there is still a long way before the material quality can be classified as suitable for devices.

As a contribution to the understanding of InN, in publication VI InN was grown by vertical flow MOVPE. In publication VII, several metal contacts were tested, and rectifying behavior was observed in Ge, Pt and annealed Al contacts.

6.1 InN growth by MOVPE

InN is a promising semiconductor for optoelectronic applications in the future. Hence, in this study we engaged on the optimisation of basic growth parameters of InN by MOVPE. Several growth temperatures and growth rates were used, in order to see their effect on the material quality.

InN was grown on nitridated c-plane sapphire substrates by vertical close-coupled showerheard (CCS) MOVPE reactor. Trimethylindium (TMIn) and ammonia (NH_3) were used as In and N precursors, respectively. To clean the surface from impurities, the substrates were annealed at 1050 ^{o}C for 10 min under hydrogen flow. After that, they were nitridated in NH_3 at 1050 ^{o}C for 30 min. Subsequently, the temperature was decreased to the growth temperature between 550 ^{o}C and 650 ^{o}C and the carrier gas was switched from H_2 to N_2.

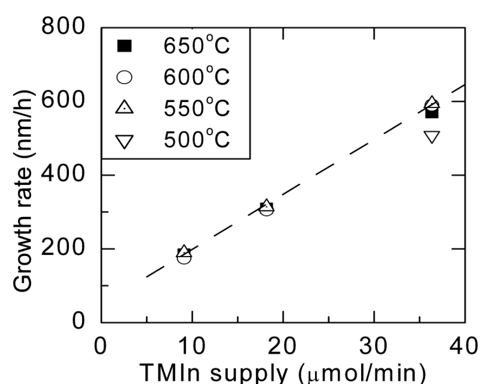

Fig. 19. Growth rate of InN as a function of TMIn molar flow supply at different growth temperatures. The V/III ratio was between 7370 and 29500.

The growth rate of InN as a function of TMIn molar flow is shown in Fig. 19. There is a linear dependence of the growth rate on the TMIn flow in the studied temperature range. Only at 500 ^{o}C, the growth rate was decreased compared to the other samples grown with the same V/III ratio. This indicates that the growth rate is not limited by NH_3 decomposition rate but by the amount of reactive In.

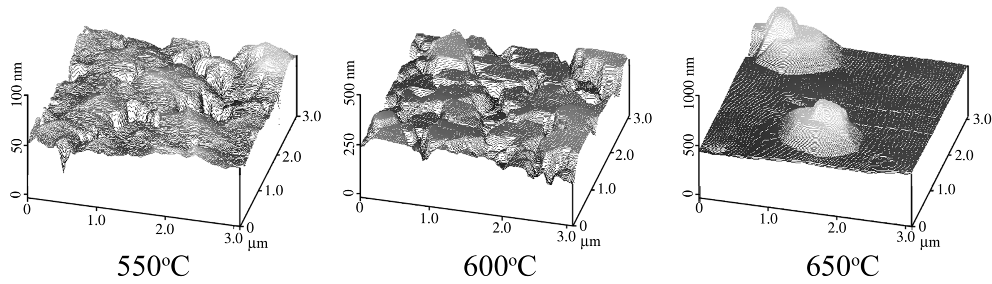

Fig. 20. AFM scans of InN film surface grown at 550, 600 and 650 °C.

In Fig. 20, the AFM scans of the InN film grown at 550 °C, 600 °C and 650 °C with the V/III ratio of 29500 are shown. The presence of 3D hexagonal shape islands on the surface can be seen. The island size increases with increasing growth temperature. The hexagonal shape is clear for the growth temperature of 650 °C, but less clear for smaller temperatures.

Hall measurements were done on the samples to determine the Hall mobility and carrier concentration. The dependence of these parameters as a function of growth temperature can be seen in Fig. 21 a). The Hall mobility increases from 100 cm^2/Vs to nearly 200 cm^2/Vs when the temperature increases from 550 °C to 650 °C. On the other hand, carrier concentration drops from 6×10^{20} to 1×10^{20} cm^{-3}. It seems that the carrier concentration and the Hall mobility are not affected by the V/III ratio. This suggest that the temperature dependence of the carrier concentration and Hall mobility is not a result from the more efficient cracking of NH_3, but from the better material quality due to higher growth temperature.

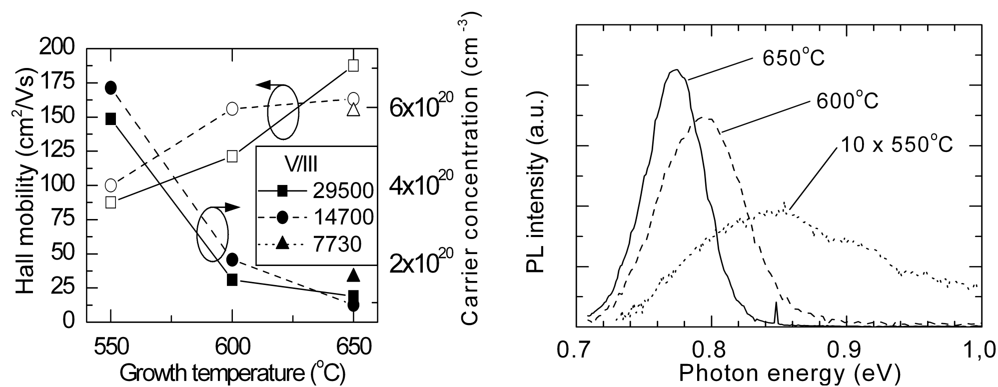

Fig. 21. a) Hall mobility and carrier concentration of the InN samples as a function of growth temperature with various V/III ratios. b) PL spectra of InN samples grown at different temperatures.

Strong support for better material quality at higher growth temperature comes also from photoluminescence (PL) measurements, as shown in Fig. 21 b). The peak intensity increases by more than tenfold and the full with at half maximum (FWHM) of the peak decreases from a 133 meV to 37 meV when the growth temperature increases from 550 ^{o}C to 650 ^{o}C. The PL spectra were not affected by different V/III ratios. It is interesting to note that the samples did not show any luminescence at 1.9 eV, which was previously thought to be the band gap energy of InN.

This study showed that InN is a difficult material to fabricate. The growth of the material at 650 ^{o}C yields the best photoluminescence spectra, the best Hall mobility values, and the lowest n-type carrier concentration. Still, the carrier concentration is very high. Similar quality as observed in other studies was achieved. However, p-type InN could not be realized by direct epitaxial growth.

6.2 Metal contacts on InN

Due to the expected applications of InN to optoelectronic devices, it is necessary to study the electrical properties of InN, which are not well known. As *p*-type InN is currently unachievable, the study of *p-n* junctions is not possible. Therefore, only a Schottky contact is suitable for studies such as DLTS, *C-V* and *I-V* measurements. Thus far, regardless of a few studies using Hg, Ti, Al or Ni that have been carried out[102,106], reliable Schottky contact had not been realised. Large lattice mismatch with the substrates, high carrier concentration, and rough surface morphology have turned out to be difficult obstacles in the quest for a Schottky contact.

The objective of this research was to gain understanding about metal contacts on InN. This was done with the following aims: a) test as many possible different metals on InN, b) study which form ohmic and which Schottky contacts, and c) in the case of Schottky ones, make *I-V* studies. During the study, it was found that Al, one of the metals tested in this study, reacts in some conditions with N to form a wide bandgap semiconductor. Hence, the idea of annealing Al contacts on InN was suggested, put in practice and reported.

In publication VII tests of several metal contacts (Au, Ag, Pt, Pd, Cu, Ni, Ge, Ti, Cr, Al) on InN were reported. Among these, only the annealed Al layer forms a reliable rectifying contact. Pt and Ge showed also some Schottky contact behavior (Fig. 22), but they were very unstable. The procedure to analyse the curves was the following. Eq. 9 can be approximated by

$$I \sim I_S \; exp(qV/nkT), \tag{40}$$

if

$$V > nkT/q. \tag{41}$$

At room temperature, $kT/q = 0.026$ eV. As n was unknown, it was necessary to estimate where the absolute current showed a linear behavior in the logarithm graph (Fig. 22). This happened around 0.06 eV. The value of I_S was estimated to be 0.001 A and 2×10^{-7} A for Ge and Pt, respectively. The linear fitting of $ln(I/I_S)$ yielded n = 1.67 and n = 0.85 for Ge and Pt respectively. This is in agreement with Eq. 41. These values should be considered with some care, because $n<1$ should not be expected. It must be remembered that the Schottky model

relies on the assumption of perfect crystals with perfect surfaces. It is clear that this is not the case here. In the future, the tunneling model could be tested, as the curves were very symmetric and the carrier concentration is high.

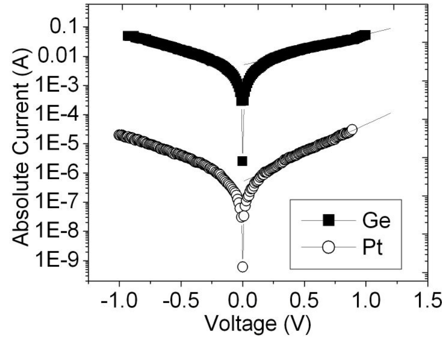

Fig. 22. Ge and Pt contact showing Schottky behavior plotted on a logarithmic scale. The linear fittings of ln (I) vs. V in the forward bias region for Ge and Pt are also shown.

In the case of the Al contact, it is possible that AlN or AlInN is formed between the semiconductor and the metal, due to N reacting with In and Al. It has been reported that Al reacts with GaN to form AlGaN and the reaction between Al and InN is also likely here[107]. It is known that AlN and GaN have stronger bonds than InN. Therefore, it is also likely that Al will react with N. If the reaction of Al and N is unavoidable, then it should be used in a profitable way to form an insulating material[108]. In the case of $Al_xIn_{1-x}N$, with x=1, the material has a wide band gap of 6.3 eV, which decreases with In content[108]. Combined with the small band gap of InN, a barrier can be formed with a rectifying behavior.

In order to see if the quality of the contacts is affected by the annealing temperature, four contacts on each InN sample, labeled pixel 1 to 4, were tested. Each set of four pixels was processed and annealed similarly with the only exception being the annealing temperature and time. Annealing was done at 300 ^{o}C, 410 ^{o}C, 500 ^{o}C and 550 ^{o}C for 1 min and at 600 ^{o}C for 24 s. Annealing up to 500 ^{o}C does not result in rectifying behavior (Fig. 23 a)). The calculated average resistances for each annealing temperature are shown in Fig. 23 b). It is possible to observe that the resistances are smaller for the sample annealed at 300 ^{o}C than for the un-annealed sample. The resistance decreases more after annealing at 410 ^{o}C. This can be seen clearly in the average resistance. It is known that annealing improves ohmic contacts due to a metal-semiconductor intermixing. The resistance increases after annealing at 500 ^{o}C, compared with the sample annealed at 410 ^{o}C, which might suggest the formation of an AlInN barrier.

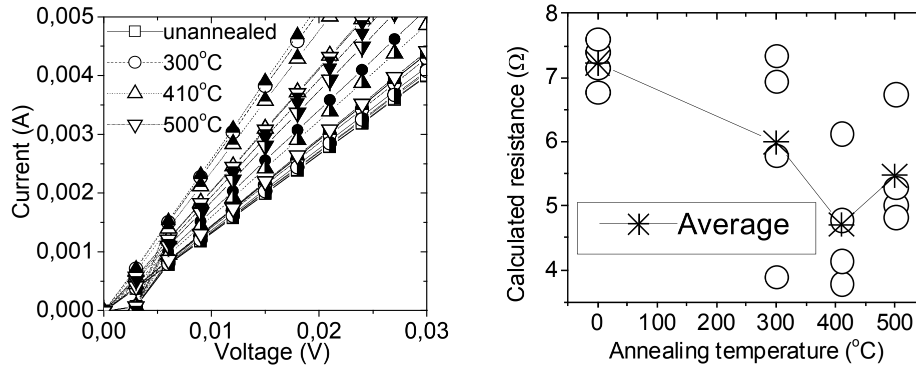

Fig. 23. a) I-V curves for 200-nm-thick annealed and un-annealed Al contacts on InN. Annealing time was 1 min. Four contacts were measured for each annealing temperature and they are represented as different shading (filled, empty, horizontally partially filled and vertically partially filled). b) Calculated resistances from the slope of the I-V curves shown in a) as a function of annealing temperature. The un-annealed samples are shown at 0 °C. The average of the resistance for each annealing temperature is also shown.

Only in the sample that was annealed at 550 °C for 1 min was rectifying behavior observed, as can be seen in Fig. 24. The order of the measurements was from low voltage ranges to high voltage ranges. For each voltage range, several measurements were done and all were identical. Interestingly, the contact at the beginning showed ohmic behavior, which became rectifying after the first measurement between –0.7 and 0.7 V was done. As the voltage range was increased, the rectifying behavior became larger. Fig. 24 suggests that the voltage provides energy, which affects the material structurally and/or energetically so that more rectifying nature is seen. These measurements were repeated several days later, and the rectifying behavior did not change, even for small voltages. Interestingly, Al contacts on GaN annealed at similar temperatures (575 °C for 10 min) have also changed their nature from ohmic to rectifying[109].

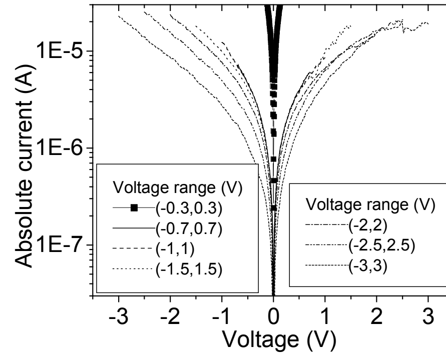

Fig. 24. I-V curves on a logarithmic scale for 200-nm-thick annealed Al contacts on InN. The annealing was performed at 550 °C for 1 min.

In conclusion, several metal contacts (Au, Ag, Pt, Pd, Cu, Ni, Ge, Ti, Cr, Al) were tested on MOVPE-grown InN. All the metals formed ohmic contact, except Pt, Ge and Al. Pt and Ge showed rectifying characteristics for voltages below –1 V. Higher voltages made them ohmic. Al contacts were ohmic for annealing temperatures of 500 °C or smaller. After annealing at 550 °C or higher temperature they showed a rectifying behavior. It is necessary to bias the voltage to –0.7 V or larger in order to change the contact behavior from ohmic to rectifying.

The stable rectifying nature of annealed Al contacts should provide a tool in the future to study this material electrically by DLTS, *I-V*, *C-V* and Hall measurements. A continuation of this study could be to study the metal contacts by SIMS, Auger spectroscopy or transmission electron microscopy (TEM). This could obtain information of the suspected AlInN interface formed in annealed Al contacts on InN.

Chapter 7

Summary

Novel nitrogen-containing III-V semiconductors have attracted a lot of attention in the last years. In addition to the obvious visible and UV light applications, another reason is their suitability for optoelectronic applications, such as telecommunication lasers and solar cells, in the 1.3 and 1.55 μm wavelength range. They have also shown promising results for electronic applications, such as transistors. Due to their novelty, many properties and especially the electrical properties are not well known.

In this thesis, an improved variant of DLTS is presented. Inductors are used to improve the acquisition of deep level parameters. It has been found that the use of the right inductors can separate DLTS signals, providing a tool to make more accurate measurements. The use of inductors also helps to determine the real series resistance and capacitance of a Schottky contact. Usually the series resistance is neglected, which causes errors for the deep level parameters. The DLTS signals can be corrected once the real resistance of the Schottky sample is known.

The DLTS technique has been used to study GaInAs. A low In composition has been used to facilitate comparison with the GaAs results. Several deep levels have been found. The samples were also annealed at several temperatures, in order to see how the deep level concentrations were affected. It was found that GaInAs has three main deep levels. One of them is not affected by thermal annealing up to 700 ^{o}C. The concentration of one level is reduced with increasing annealing temperature. The concentration of both of these levels decreases when annealed at 750 ^{o}C. The third deep level has a small concentration, which is not affected by annealing. Further study to understand the structural origin of the deep levels and their effect on device performance is needed.

GaInNAs is expected to have a deep impact in optoelectronics applications, as it can be grown lattice matched to GaAs, if the correct ratio of In and N compositions is used. In this thesis GaInNAs has been studied by DLTS. Low In and N compositions have been used to facilitate comparison with the GaAs results. Two samples were studied, one with medium doping and the other one with high doping. For the medium doped sample, one main deep level appears for the as-grown sample. The concentration of this level decreases as the annealing temperature increases. Four deep levels appear as the annealing temperature is

increased. The concentrations of all these levels increase with increasing temperature. Regarding the highly doped sample, only one deep level appears, and its concentration decreases with increasing temperature. The DLTS parameters of these levels are compared with the known deep levels of GaAs. As in the case of GaInAs, deep levels can have a major impact on the optical efficiency of GaInNAs.

In the future, optical and structural studies of GaInAs and GaInNAs should provide insight on the nature of these deep levels, like their origin, local composition and structure. PL studies can yield information about the radiative nature of the levels. In that case, time-resolved PL (TRPL) might provide information on the emission rates. This can be compared with results obtained by ODLTS measurements.

InN samples were grown at different temperatures and with different V/III ratios. It was found that the V/III ratio does not have a major impact on the material properties, but the growth temperature has. The best material was obtained at the growth temperature of 650°C: it showed lower carrier concentrations and higher Hall mobilities than samples grown at other temperatures. Also, the PL peak was the sharpest and most intense. With this InN sample, several metal contacts were tested. Due to the novelty of InN, systematic studies of the metal contacts on InN cannot be found in the literature. It was found that Pt and Ge make Schottky contacts, which are not very reliable. Al contacts were annealed, and when the annealing temperature was 550 ^{o}C, they showed rectifying behavior. Schottky contacts on InN, in general, might provide deeper insight on the electrical properties of InN. *I-V, C-V* and DLTS measurements could provide information on, *e.g.*, the carrier concentration profile, barrier height, Richardson constant and deep levels.

References

[1] O. B. Shchekin and D. G. Deppe, *1.3 μm InAs quatum dot laser with T_o=161 K from 0 to 80°C*, Appl. Phys. Lett. **80**, 3277 (2002).

[2] M. Weyers, M. Sato and H. Ando, *Red shift of photoluminescence and absorption in dilute GaAsN alloy layers*, Jpn. J. Appl. Phys. **31**, L853 (1992).

[3] M. Kondow, K. Uomi, A. Niwa, T. Kitatani, S. Watahiki and Y. Yazawa, *GaInNAs: a novel material for long-wavelength-range laser diodes with excellent high-temperature performance*, Jpn. J. Appl. Phys. **35**, 1273 (1996).

[4] J. Wu, W. Walukiewicz, K. M. Yu, J. W. Ager III, E. E. Haller, H. Lu, W. J. Schaff, Y. Saito and Y. Nanishi, *Unusual properties of the fundamental band gap of InN,* Appl. Phys. Lett. **80**, 3967 (2002).

[5] T. Matsuoka, H. Okamoto, M. Nakao, H. Harima and E. Kurimoto, *Optical bandgap energy of wurtzite InN*, Appl. Phys. Lett. **81**, 1246 (2002).

[6] S. J. Pearton, F. Ren, A. P. Zhang and K. P. Lee, *Fabrication and performance of GaN electronic devices*, Mat. Sci. Eng. **R30**, 55 (2000).

[7] S. R. Kurtz, A. A. Allerman, E. D. Jones, J. M. Gee, J. J. Banas and B. E. Hammons, *InGaAsN solar cells with 1.0 eV band gap, lattice matched to GaAs*, Appl. Phys. Lett. **74**, 729 (1998).

[8] D. J. Friedman, J. F. Geisz, S. R. Kurtz and J. M. Olson, *1-eV solar cells with GaInNAs active layer*, J. Cryst. Growth **195**, 409 (1998).

[9] R. J. Kaplar, D. Kwon, S. A. Ringel, A. A. Allerman, S. R. Kurtz, E. D. Jones and R. M. Sieg, *Deep levels in p- and n-type InGaAsN for high-efficiency multi-junction III-V solar cells*, Solar Energy Materials & Solar Cells **69**, 85 (2001).

[10] S. Averin, R. Sachot, J. Hugi, M. de Fays and M. Ilegems, *Two-dimensional device modeling and analysis of GaInAs metal-semiconductor-metal photodiode structures*, J. Appl. Phys. **80**, 1553 (1996).

[11] Peter, Y. Yu and Manuel Cardona, *Fundamentals of Semiconductors, Physics and Materials Properties*, Springer, (Germany) 2003.

[12] A. A. Bergh and P. J. Dean, *Light-emitting Diodes*, Proc. IEEE **60**, 156 (1972).

[13] Leonard I. Grossweiner, *A Note on the Analysis of First-Order Glow* Curves, J. Appl. Phys. **24**, 1306 (1953); R. H. Bube, Photoconductivity of solids, Wiley, New York, 1960.

[14] D. L. Losee, *Admittance spectroscopy of deep impurity levels: ZnTe Schottky barriers*, Appl. Phys. Lett. **21**, 54 (1974).

[15] A. Rose, *An outline of some photoconductive processes*, RCA Rev. **12**, 362 (1951); H. B. DeVore, *Gains, response times, and trap distributions in powder photoconductors,* RCA Rev. **20**, 79 (1959).

[16] John Lambe, *Recombination Processes in Cadmium Sulfide*, Phys. Rev. **98**, 985 (1955); Richard H. Bube, *Comparison of Surface-Excited and Volume-Excited Photoconduction in Cadmium Sulfide Crystals*, Phys. Rev. **101**, 1668 (1956).

[17] R. W. Smith and A. Rose, *Space-Charge-Limited Currents in Single Crystals of Cadmium Sulfide*, Phys. Rev. **97**, 1531 (1955); A. Rose, *Space-Charge-Limited Currents in Solids*, Phys. Rev. **97**, 1538 (1955); Murray A. Lampert, *Simplified Theory of Space-Charge-Limited Currents in an Insulator with Traps*, Phys. Rev. **103**, 1648 (1956).

[18] R. Williams, *Determination of Deep Centers in Conducting Gallium Arsenide*, J. Appl. Phys. **37**, 3411 (1966).

[19] C. T. Sah, W. W. Chan, H. S. Fu and J. W. Walker, *Thermally Stimulated Capacitance (TSCAP) in p-n Junctions*, Appl. Phys. Lett. **20**, 193 (1972), C. T. Sah and J. W. Walker, *Thermally stimulated capacitance for shallow majority-carrier traps in the edge region of semiconductor junctions*, Appl. Phys. Lett. **22**, 384 (1973).

[20] D. V. Lang, *Deep-level transient spectroscopy: A new method to characterize traps in semiconductors*, J. Appl. Phys. **45**, 3023 (1974).

[21] W. Schockley and W. T. Read, *Statistics of the recombinations of holes and electrons,* Phys. Rev. **87**, 835 (1952).

[22] P. Blood and J. W. Orton, *The electrical characterization of semiconductors*, Rep. Prog. Phys., **41**, 158 (1978).

[23] S. M. Sze, *Physics of semiconductor devices,* John Wiley, (USA) 1981.

[24] Avishay Katz, *Indium Phosphide and Related Materials: Processing, Technology and Devices*, Artech house, Inc, USA, 1992.

[25] P. Blood and J. W. Orton, *The electrical characterization of semiconductors: majority carriers and electron states,* Academic Press, UK, 1992.

[26] L. Stolt, K. Bohlin, *Deep-level transient spectroscopy measurements using high Schottky barriers*, Solid-state electron. **28**, 1215 (1985); F. D. Auret and M. Nel, *Detection of minority-carrier defects by deep level transient spectroscopy using Schottky barrier diodes*, J. Appl. Phys. **61**, 2546 (1987).

[27] W. Meyer and H. Neldel, *Uber die Beziehungen zwischen der Energiekonstanten und der Mengenkonstanten a in der LeitwertsTemperaturformel bei oxydischen Halbleitern*, Z. Tech. Phys. **12**, 288 (1937).

[28] R. W. Keyes, *Volumes of Activation for Diffusion in Solids*, J. Chem. Phys. **29**, 467 (1958).

[29] J.-P. Crine, *A new analysis of the results of thermally stimulated measurements in polymers,* J. Apply. Phys. **66**, 1308 (1989).

[30] K. Miyairi, Y. Othta and M. Ieda*, The compensation law in electric conduction and dielectric relaxation for polyvinyl chloride,* J. Phys. D **21**, 1519 (1988).

[31] H. Overhof and P. Thomas, *Electronic Transport in Hydrogenated Amorphous Semiconductors* (Springer-Verlag, New York, 1989).

[32] S. W. Johnston, R. S. Crandall and A. Yelon, *Evidence of the Meyer-Neldel rule in InGaAsN alloys and the problem of determining trap capture cross sections*, Appl. Phys. Lett. **83**, 908 (2003).

[33] M. C. Chen, D. V. Lang, W. C. Dautremont-Smith, A. M. Sergent and J. P. Harbison, *Effects of leakage current on deep level transient spectroscopy*, Appl. Phys. Lett. **44**, 790 (1984).

[34] H. Lefevre and M. Schulz, *Double correlation technique (DDLTS) for the analysis of deep levels profiles in semiconductors*, Appl. Phys. **12**, 45 (1977).

[35] N. M. Johnson, D. J. Bartelink, R. B. Gold and J. F. Gibbons, *Constant-capacitance DLTS measurement of defect-density profiles in semiconductor*, J. Appl. Phys. **50**, 4828 (1979).

[36] W. Götz, N. M. Johnson, R. A. Street, H. Amano and I. Akasaki, *Photoemission capacitance transient spectroscopy of n-type* GaN, Appl. Phys. Lett. 66, 1340 (1995).

[37] S. Weiss and R. Kassing, *Deep level transient fourier spectroscopy (DLTFS)-A technique for the analysis of deep level properties*, Solid-State Electronics **31**, 1733 (1988); L. Dobaczewski, P. Kaczor, I. D. Hawkings and A. R. Peaker, *Laplace transform deep-level transient spectroscopic studies of defects in semiconductors*, J. Appl. Phys. **76**, 194 (1994).

[38] H. Okushi and Y. Tokumaro, *Isothermal Capacitance Transient Spectroscopy for Determination of Deep Level Parameters*, Jpn. J. Appl. Phys. **19**, L335 (1980).

[39] C. D. Beling, *New defect spectroscopies*, Appl. Surf. Science **194**, 224 (2002).

[40] H. K. Henish, *Semiconductors Contacts: An Approach to Ideas and Models,* Oxford University Press, (New York, USA) 1985.

[41] A. Broniatowski, A. Bloose, P. C. Srivastava and J. C. Bourgoin, *Transient capacitance measurements on resistive samples*, J. Appl. Phys. **54**, 2907 (1983).

[42] J. Werner, A. F. J. Levi, R. T. Tung, M. Anzlowar and M. Pinto, *Origin of the Excess Capacitance at Intimate Schottky Contacts,* Phys. Rev. Lett. **60**, 53 (1988).

[43] R. J. Kaplar, D. Kwon, S. A. Ringel, A. A. Allerman, Steven R. Kurtz, E. D. Jones and R. M Sieg, *Deep levels in p- and n-type InGaAsN for high efficiency multi-junction III-V solar cells,* Solar Energy Mater. Sol. Cells **69**, 85 (2001).

[44] So Tanaka, A. Moto, M. Takahashi, T. Tanabe and S. Takagishi, *Spatial distribution of deep level traps in GaNAs crystals*, J. Crys. Growth **221**, 467 (2000).

[45] Assem M. Bakry and Salah Darweesh, *Deep level defects in n- and p-type Fe implanted InP*, Physica A **242**, 161 (1997).

[46] H. Ishii, T. Shinagawa, S. Tanaka and T. Okumura, *Characterization of oxygen-related defects in p-$Al_{0.3}Ga_{0.7}As$ by DLTS*, J. Crys. Growth **210**, 242 (2000).

[47] M. S. Abrahams, R. Braunstein and F.D. Rosi, *Thermal, electrical and optical properties of (In, Ga)As alloys*, J. Phys. Chem. Solids **10**, 204 (1959).

[48] F. D. Rosi, J. P.Dismukes and E. F. Hockings, *Semiconductor materials for thermoelectric power generation up to 700 C*, Elec. Eng. **79**, 450 (1960); F. D. Rosi, E. F. Hockings and N. E. Lindenblad, *Semiconducting materials for thermoelectric power generation*, RCA Rev. **22**, 82 (1961)).

[49] E. F. Hockings, I. Kudman, T. E. Seidel, C. M Schmelz and E. F. Steigmeier, *Thermal and Electrical Transport in InAs-GaAs Alloys*, J. Appl. Phys., **37**, 2879 (1966).

[50] I. Melngailis, *Maser action in InAs diodes*, Appl. Phys. Lett. **2**, 176 (1963).

[51] N. S. Rytova, E. V. Solov΄eva and M. G. Mil΄vidskii, *Mechanism of the interaction of isovalent In and Sb impurities with the system of point defects in GaAs*, Sov. Phys. Semicond. **16**, 951 (1982).

[52] E. V. Solov΄eva, N. S. Rytova, M. G. Mil΄vidskii and N. V. Ganina, *Electrical properties of gallium arsenide doped with isovalent impurities (GaAs:Sb, GaAs:In)*, Sov. Phys. Semicond. **15**, 1243 (1981).

[53] G. Jacob, M. Duseaux, J. P. Farges, M. M. B. van den Boom and P. J. Roksnoer, *Dislocation-free GaAs and InP crystals by isoelectronic doping*, J. Cryst. Growth **61**, 417 (1983).

[54] H. M. Hobgood, R. N. Thomas, D. L. Barrett, G. W. Eldrige, M. M. Sopira and M. C. Driver, *Large Diameter, Low Dislocation In-Doped GaAs: Growth, Characterization and Implications for FET Fabrication*, Proced. Intern. Conf. on Semi-Insul. III-V Mat., edited by D.C.Look and J. S. Blakemore (Shive, England) 1984, p. 149.

[55] M. Duseaux and S. Martin, *Growth and Characterization of Large Dislocation-Free GaAs Crystals for Integrated Circuits Applications,* Proced. Intern. Conf. on Semi-Insul. III-V Mat., edited by D.C.Look and J. S. Blakemore (Shive, England) 1984, p. 111.

[56] H. Ehrenreich and J. P. Hirth, *Mechanism for dislocation density reduction in GaAs crystals by indium addition*, Appl. Phys. Lett. **46**, 668 (1985).

[57] H. Beneking, P. Narozny and N. Emeis, *High quality epitaxial GaAs and InP wafers by isoelectronic doping*, Appl. Phys. Lett. **47**, 828 (1985).

[58] P. Narozny and H. Beneking, *High-quality GaAs Schottky diodes fabricated by strained layer epitaxy*, Electr. Lett., **21**, 1050 (1985).

[59] H. Beneking, P. Narozny, P. Roentgen and M. Yoshida, *Enhanced carrier lifetime and diffusion length in GaAs by strained-layer MOCVD*, Electr. Dev. Lett. **7**, 101 (1986).

[60] Hiroaki Takeuchi, Masanori Shinohara, Kunishige Oe, *An In-Doped Dislocation-Free GaAs Layer Grown by MBE on an In-Doped GaAs Substrate*, Jpn. J. Appl. Phys. **25**, L303 (1986).

[61] Utpal Das, Pallab K. Bhattacharya and Sunanda Dhar, *Low-loss optical waveguides made with molecular beam epitaxy* $In_{0.012}Ga_{0.988}As$ *and* $In_{0.2}Ga_{0.8}As$ *superlattices,* Appl. Phys. Lett. **48**, 1507 (1986).

[62] M. Missous, K. E. Singer and D. J. Nicholas, *Electrical properties of Indium doped GaAs layers grown by MBE*, J. Cryst. Growth **81**, 314 (1987).

[63] W. C. Mitchel, Gail J. Brown, David W. Fischer, P. W. Yu and Joseph E. Lang, *Characterization of the intrinsic double acceptor in undoped p-type gallium arsenide*, J. Appl. Phys. **62**, 2320 (1987).

[64] S. R. Smith, A. O. Evwaraye, and W. C. Mitchel, *Observation of a deep level due to In doping in p-type GaAs*, J. Appl. Phys. **65**, 1130 (1989).

[65] Pallab K. Bhattacharya, Sunanda Dhar, Paul Berger and Feng-Yuh Juang, *Low defect densities in molecular beam epitaxial GaAs achieved by isoelectronic In doping*, Appl. Phys. Lett. **49**, 470 (1986).

[66] D. E. Ioannou, Y. J. Huang and A. A. Illiadis, *Deep states and misfit dislocations in indium-doped GaAs layers grown by molecular beam epitaxy*, Appl. Phys. Lett. **52**, 2258 (1988).

[67] A. Mircea, A. Mitonneau, J. Hallais and M. Jaros, *Study of the main electron trap in* $Ga_{1-x}In_xAs$ *alloys*, Phys. Rev. B **16**, 3665 (1977).

[68] T. Zhang, T. W. Sigmon, K. H. Weiner and P. G. Carey, *Defect-induced Schottky barrier height modification by pulsed laser melting of GaAs*, Appl. Phys. Lett. **55**, 580 (1989).

[69] A. Y. Du, M. F. Li, T. C. Chong, K. L. Teo, W. S. Lau and Z. Zhang, *Dislocations and related traps in p-InGaAs/GaAs lattice-mismatched* heterostructures, Appl. Phys. Lett. **69**, 2849 (1996).

[70] Liwu Lu, Songlin Feng, Jiben Liang, Zhanguo Wang, J. Wang, Y. Wang and Weikun Ge, *Characterization of deep centers in AlGaAs/InGaAs/GaAs pseudomorphic HEMT structures grown by molecular beam epitaxy and hydrogen treatment*, J. Cryst. Growth **169**, 637 (1996).

[71] T. Wosinski, O. Yastrubchak, A. Makosa and T. Figielski, *Deep level defets at lattice-mismatched interfaces in GaAs-based heterojunctions*, J. Phys. Condens. Matter. **12**, 10153 (2000).

[72] O. Yastrubchak, T. Wosinski, A. Makosa, T. Figielski and A. L. Toth, *Capture kinetics at deep-level defects in lattice-mismatched GaAs-based heterostructures*, Physica B, **308**, 757 (2001).

[73] I. Dermoul, F. Chekir, M. Ben Salem, A. Kalboussi and H. Maaref, *Deep level investigation in AlGaAs/InGaAs/GaAS cryelectronic MODFET*, Solid-St. Electr. **45**, 1059 (2001).

[74] M. J. Matragano, G. P. Watson, D. G. Ast, T. J. Anderson and B. Pathangey, *Passivation of deep level states caused by misfit dislocations in InGaAs on patterned GaAs*, Appl. Phys. Lett. **62**, 1417 (1993).

[75] L. Panepinto, U. Zeimer, W. Seifert, M. Seibt., F. Bugge, M. Weyers and W. Schröter, *Temperature dependent EBIC and deep level transient spectroscopy investigation of different types of misfit-dislocations at MOVPE grown GaAs/InGaAs/GaAs-single-quantum wells*, Mat. Sci. and Eng. B **42**, 77 (1996).

[76] N. Sghaier, S. Bouzgarrou, M. M. Ben Salem, A. Souifi, A. Kalboussi and G. Guillot, *I-V anomalies on InAlAs/InGaAs/InP HFETs and deep levels investigations*, Mat. Sci. and Eng. B **121**, 178 (2005).

[77] A. Z. Wang and W. A. Anderson, *Influence of a single InGaAs quantum well on current transport and deep levels in GaAs*, Sol.-Stat. Electr. **38**, 673 (1995).

[78] M. M. Sobolev, I. V. Kochnew, V. M. Lantratov, N. A. Cherkashin and V. V. Emtsev, *Hole and electron traps in the InGaAs/GaAs heterostructures with quantum dots*, Phys. B **273**, 959 (1999).

[79] W-P. Hong, C. Caneau, J. R. Hayes, R. Bhat, G. K. Chang, C. Nguyen and Y. H. Jeong, *Effects of in situ treatment on InGaAs/InP heterointerfaces produced by organometallic chemical vapor deposition regrowth*, J. Appl. Phys. **70**, 502 (1991).

[80] G. J. Shaw, S. R. Messenger, R. J. Walters and G. P. Summers, *Radiation-induced reverse dark currents in* $In_{0.53}Ga_{0.47}As$ *photodiodes*, J. Appl. Phys. **73**, 7244 (1993).

[81] G. J. Shaw, R. J. Walters, S. R. Messenger and G. P. Summers, *Time dependence of radiation-induced generation currents in irradiated InGaAs photodiodes*, J. Appl. Phys. **74**, 1629 (1993).

[82] B. Srocka, H. Scheffler and D. Bimberg, *Rhodium- and iridium-related deep levels in* $In_{0.53}Ga_{0.47}As$, Appl. Phys. Lett. **64**, 2679 (1994).

[83] Wei Gao, Paul R. Berger, Mathew H. Ervin, Jagadeesh Pamulapati, Richard T. Lareau and Stephen Schauer, *Liquid phase epitaxial growth of InGaAs on InP using rare-earth-treated melts*, J. Appl. Phys. **80**, 7094 (1996).

[84] Yoshifumi Takanashi and Naoto Kondo, *Deep trap in InGaAs grown by gas source molecular beam epitaxy*, J. Appl. Phys. **85**, 633 (1999).

[85] J. Samitier, J. R. Morante, A. Cornet, A. Herms, P. Roura and A. Pérez, *Optical isothermal transient spectroscopy: application to the boron implantation in GaAs,* Mater. Sci. Forum **10-12**, 539 (1986).

[86] Masahiko Kondow, Kazuhia Uomi, Atsuko Niwa, Takeshi Kitatani, Seiji Watahiki and Yoshiaki Yazawa, *GaInNAs: A Novel Material for Long-Wavelength-Range Laser Diodes with Excellent High-Temperature Performance*, Jpn. J. Appl. Phys. **35**, 1273-1275 (1996).

[87] M. Kondow, K. Uomi, K. Hosomi and T. Mozume, *Workbook 8th. Int. Conf. Molecular Beam Epitaxy, Osaka*, 323 (1994).

[88] M. Kondow, S. Natatsuka, T. Kitatani, Y. Yazawa and M. Okai, *Room-temperature continuous-wave operation of GaInNAs/GaAs laser diode*, Elec. Lett. **32**, 2244 (1996).

[89] M. C. Larson, M. Kondow, T. Kitatani, K. Tamura, Y. Yazawa and M. Okai, *Photopumped Lasing at 1.25 μm of GaInNAs-GaAs Multiple-Quantum-Well Vertical-Cavity Surface-Emitting Lasers*, IEEE Photonics Tech. Lett. **9**, 1549 (1997).

[90] M. Kondow, T. Kitatani, M. C. Larson, K. Nakahara, K. Uomi and H. Inoue, *Gas-source MBE of GaInNAs for long-wavelength laser diodes*, J. Crystal Growth **188**, 255 (1998).

[91] S. J. Pearton, F. Ren, A. P. Zhang and K. P. Lee, *Fabrication and performance of GaN electronic devices*, Mater. Sci. Eng. **R30**, 55 (2000).

[92] D. J. Friedman, J. F. Geisz, S. R. Kurtz and J. M. Olson, *1-eV solar cells with GaInNAs active layer*, J. Cryst. Growth **195**, 409 (1998).

[93] S. R. Kurtz, A. A. Allerman, E. D. Jones, J. M. Gee, J. J. Banas and B. E. Hammons, *InGaAsN solar cells with 1.0 eV band gap, lattice matched to GaAs*, Appl. Phys. Lett. **74**, 729 (1999).

[94] R. J. Kaplar, D. Kwon, S. A. Ringel, A. A. Allerman, S. R. Kurtz, E. D. Jones and R. M. Sieg, *Deep levels in p- and n-type InGaAsN for high-efficiency multi-junction III-V solar cells*, Solar Energy Materials & Solar Cells **69**, 85 (2001).

[95] G. M. Martin, A. Mitonneau and A. Mircea, *Electron traps in bulk and epitaxial GaAs crystals*, Electronics Lett., **13**, 191 (1977).

[96] A. Y. Polyakov, N. B. Smirnov, A. V. Govorkov, Andrei E. Botchkarev, Nicole N. Nelson, M. M. E. Fahmi, James A. Griffin, Arif Khan, S. Noor Mohammad, D. K. Johnstone, V. T. Bublik, K. D. Chsherbatchev, M. I. Voronova and V. S. Kasatochkin, *Studies of deep centers in dilute GaAsN and InGaAsN films grown by molecular beam epitaxy*, Solid-State Electron **46**, 2155 (2002).

[97] H. F. Liu, S. Karirinne, C. S. Peng, T. Jouhti, J. Konttinen and M. Pessa, *In situ annealing effect on the structural properties of near-surface GaInNAs/GaAs quantum wells*, J. Cryst. Growth **263**, 171 (2004).

[98] R. R. Sumathi, M. Udhayasankar, J. Kumar, P. Magudapathy and K. G. M. Nair, *Effect of proton irradiation on the characteristics of GaAs Schottky barrier diodes,* Physica B **308**, 1209 (2001).

[99] Franz Fischer and Fritz Schröter, *Über neue Metall-Stickstoff-Verbindungen und ihre Stabilität an der Hand des periodischen Systems*, Ber. Dtsch. Chem. Ges. **43**, 1465 (1910).

[100] K. S. A. Butcher and T. L. Tansley, *InN, latest development and a review of the band-gap controversy*, Superlat. And Microstruc. **38**, 1 (2005).

[101] T. L. Tansley and C. P. Foley, *Optical band gap of indium nitride,* J. Appl. Phys. **59**, 3241 (1986).

[102] J. Wu, W. Walukiewicz, K. M. Yu, J. W. Ager III, E. E. Haller, H. Lu, W. J. Schaff, Y. Saito and Y. Nanishi, *Unusual properties of the fundamental band gap of InN*, Appl. Phys. Lett. **80**, 3967 (2002).

[103] Takashi Matsuoka, Hiroshi Okamoto, Masashi Nakao, Hiroshi Harima and Eiji Kurimoto, *Optical bandgap energy of wurtzite InN*, Appl. Phys. Lett. **81**, 1246 (2002).

[104] Ashraful Ghani Bhuiyan, Akihiro Hashimoto and Akio Yamamoto, *Indium nitride (InN): A review on growth, characterization, and properties*, J. Appl. Phys. **94**, 2779 (2003).

[105] B. Monemar, P. P. Paskov and A. Kasic, *Optical properties of InN – the bandgap question*, Superlat. And Microstruc. **38**, 38 (2005).

[106] W. J. Schaff, H. Lu, J. Hwang and H. Wu: *Growth of InN for Heterojunction Field Effect Transistor Applications by Plasma Enchanced MBE,* IEEE (New York, USA) 2000, p. 225.

[107] S. J. Pearton, J. C. Zolper, R. J. Shul and F. Ren: *GaN: Processing, defects, and devices*, J. Appl. Phys. **86**, 1 (1999).

[108] Z. An, Ch. Men, Z. Xu, P. Chu and Ch. Lin: *Electrical properties of AlN thin films prepared by ion beam enhanced deposition*, Surf. Coat. Technol. **196**, 130 (2005).

[109] J. S. Foresi and T. D. Moustakas: *Metal contacts to gallium nitride*, Appl. Phys. Lett. **62**, 2859 (1993).

ISBN 978-951-22-8637-9
ISBN 978-951-22-8638-6 (PDF)
ISSN 1795-2239
ISSN 1795-4584 (PDF)